Phase Retrieval with Application to Optical Imaging

Yoav Shechtman*†, Yonina C. Eldar‡, Oren Cohen*, Henry N. Chapman§¶‖, Jianwei Miao** and Mordechai Segev*

*Department of Physics Technion, Israel Institute of Technology, Israel 32000

†Department of Chemistry, Stanford University, Stanford, California 94305, USA

‡Department of Electrical Engineering, Technion, Israel Institute of Technology, Israel 32000

§Center for Free-Electron Laser Science, DESY, Notkestrasse 85, 22607 Hamburg, Germany

¶University of Hamburg, Luruper Chaussee 149, 22761 Hamburg, Germany

‖Center for Ultrafast Imaging, 22607 Hamburg, Germany

**Department of Physics and Astronomy, and California NanoSystems Institute, University of California, Los Angeles, CA 90095, USA

Email: yoavsh@stanford.edu

I. Introduction

The problem of phase retrieval, namely – the recovery of a function given the magnitude of its Fourier transform - arises in various fields of science and engineering, including electron microscopy, crystallography, astronomy, and optical imaging. Exploring phase retrieval in optical settings, specifically when the light originates from a laser, is natural, because optical detection devices (e.g., ccd cameras, photosensitive films, the human eye) cannot measure the phase of a light wave. This is because, generally, optical measurement devices that rely on converting photons to electrons (current) do not allow direct recording of the phase: the electromagnetic field oscillates at rates $\sim 10^{15}$ Hz, which no electronic measurement devices can follow. Indeed, optical measurement / detection systems measure the photon flux, which is proportional to the magnitude squared of the field, not the phase. Consequently, measuring the phase of optical waves (electromagnetic fields oscillating at 10^{15} Hz and higher) involves additional complexity, typically by interfering it with another (known) field, in the process of holography.

Interestingly, electromagnetic fields do have some other features which make them amenable for algorithmic phase retrieval: their far-field corresponds to the Fourier transform of their near-field. More specifically, given a "mask" that super-imposes some structure (an image) on a quasi-monochromatic coherent field at some plane in space, the electromagnetic field structure at a large enough distance from that plane is given by the Fourier transform of the image multiplied by a known quadratic phase factor. Thus, measuring the *far-field*, magnitude and phase, would facilitate recovery of the optical image (the wavefield). However, as noted above, the optical phase cannot be measured directly by an electronic detector. Here is where algorithmic phase retrieval comes into play, offering a means for recovering the phase given the measurement of the magnitude of the optical far-field and some prior knowledge.

The purpose of this review article is to provide a contemporary review of phase retrieval in optical imaging. It begins with historical background section that also explains the physical setting, followed by a section on the mathematical formulation of the problem. The fourth section discusses existing algorithms, while the fifth section describes various contemporary applications. The last section discusses additional physical settings where algorithmic phase retrieval is important, identifies current challenges and provides a long term vision. This review article provides a contemporary overview of phase retrieval in optical imaging, linking the relevant optical physics to the signal processing methods and algorithms. Our goal is to describe the current state of the art in this area, identify challenges, and suggest vision and areas where signal processing methods can have a large impact on optical imaging and on the world of imaging at large, with applications in a variety of fields ranging from biology and chemistry to physics and engineering.
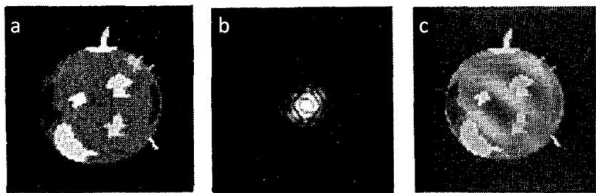
Figure 1. Numerical 2D phase retrieval example, adapted from Fienup's 1978 paper [2]. (a) Test object. (b) Fourier magnitude (c) Reconstruction results (using HIO - see Fig. 4b for details)

II. HISTORICAL BACKGROUND

Algorithmic phase retrieval offers an alternative means for recovering the phase structure of optical images, without requiring sophisticated measuring setups as in holography. These approaches typically rely on some advanced information in order to facilitate recovery. Back in 1952, Sayre envisioned, in the context of crystallography, that the phase information of a scattered wave may be recovered if the intensity pattern at and between the Bragg peaks of the diffracted wave is finely measured [1]. In crystallography, the material structure under study is periodic (a crystal), hence the far-field information contains naturally strong peaks reflecting the Fourier transform of the periodic information. Measuring the fine features in the Fourier transform enabled the recovery of the phase in some simple cases. Twenty six years later, in 1978, Fienup developed algorithms for retrieving phases of 2D images from their Fourier modulus and constraints such as non-negativity, and a known support of the image [2] (See Fig. 1). In the early eighties, the idea of phase retrieval created a flurry of follow up work, partly because those times signified great hope for realizing an optical computer, of which phase retrieval was supposed to be a key ingredient. However, in the 1980s and 1990s, with the understanding that an optical computer is unrealistic, the interest in algorithmic phase retrieval diminished. Towards the end of the millennium, optical phase retrieval started to come back into contemporary optics research, with the interest arising from a completely different direction: the community of researchers experimenting with X-ray imaging, where new X-ray sources (undulators and synchrotrons) were developed. The wide-spread interest of this field was mainly generated by the first experimental recording and reconstruction of a continuous diffraction pattern (Fourier magnitude squared) of a non-crystalline (non-periodic) test object by Miao and collaborators in 1999 [3].

The reasons for the revival of optical phase retrieval, in 1999, were actually quite subtle. One goal of optical imaging systems is to increase resolution, that is, to image smaller and smaller features. But, as known since Ernst Abbe's work in 1873, the highest attainable resolution in diffraction imaging (so-called the *diffraction limit*) is comparable to the wavelength of the light. For visible light, this diffraction limit corresponds to fraction of microns. Consequently, features on the molecular scale cannot be viewed with visible light in a microscope. One could argue then, why not simply use electromagnetic waves of a much shorter wavelength, say, in the hard X-ray regime, where the wavelength is comparable to atomic resolution? The reason is that lens-like devices and other optical components in this spectral region suffer from very large aberrations and are very difficult to make due to fact that refractive indices of materials in this wavelength regime are close to one. On the other hand, algorithmic phase retrieval is of course not limited by the quality of lenses; however it requires very low noise detectors.

An additional problem is that as resolution is improved (that is, as voxel elements in the recovered image are smaller in size), the number of photons per unit area must obviously increase to provide a reasonable SNR. This means that the required exposure time to obtain a given signal level must increase as $(1/d)^4$, with d being the resolution length, assumed to be larger than atomic scales [4]. This, in turn, creates another problem: X-ray photons are highly energetic. The atomic cross section for photoabsorption is usually much higher than for elastic scattering, meaning that for every photon that contributes to the diffraction pattern (the measured Fourier magnitude), a considerable greater number of photons are absorbed by the sample. This energy dissipates in the sample first by photoionisation and the breakage of bonds, followed by a cascade of collisional ionisation by free electrons and, at longer timescales, a destruction of the sample due to radiolysis, heating, or even ablation of the sample. Such radiation damage hinders the ability to recover the structure of molecules: the measured far-field intensity (Fourier magnitude) also reflects the structural damages, rather than providing information about the true molecular structure [5]. A solution to this problem was suggested by Solem and Chapline in the 1980's. They proposed to record images (or holograms in their case) with pulses that are shorter than the timescale for the X-ray damage to manifest itself at a particular resolution. They predicted that picosecond pulses would be required to image at nanometer length scales [6]. Towards the late nineties, with the growing promise in constructing X-ray lasers that generate ultrashort pulses on the femtosecond scale, it was suggested that such pulses could even outrun damage

processes at atomic length scales[7]. However, forming a direct image in this way would still require high quality optical components (lenses, mirrors) in the X-ray regime, which do not currently exist. This is because creating lenses for the hard X-ray wavelength regime requires fabrication at picometer resolution, much smaller even than the Bohr radius of atoms. Likewise, while mirrors for X-rays do exist, their best resolution is on the scale of many nanometers, much larger than the features one would want to resolve in imaging of molecules, for example.

The difficulties outlined above in direct X-ray imaging leave no choice but to use alternative methods to recover the structure of nanometric samples. Here is where phase retrieval can make its highest impact. Placing an area detector far enough from the sample to record the far-field diffraction intensity (which is approximately proportional to the squared magnitude of the Fourier transform of the image, if the coherence length of the X-ray wave is larger than the sample size [8], [9]), together with appropriate constraints on the support of the sample, enable the recovery of the image at nanometric resolution. Indeed, the phase information has been shown numerically and experimentally to be retrieved in this fashion in various examples [2], [10], [11], [12], [13], [14]. The combination of X-ray diffraction, oversampling and phase retrieval has launched the currently very active field called *Coherent Diffraction Imaging* or CDI [3]. In CDI, an object is illuminated with a coherent wave, and the far field diffraction intensity pattern (corresponding to the Fourier magnitude of the object) is measured. The problem then is to recover the object from the measured far-field intensity (See box on Coherent Diffractive Imaging and Fig. 2 within). Since its first experimental demonstration, CDI has been applied to image a wide range of samples using synchrotron radiation [8], [15], [16], [17], [18], [19], [20], [21], X-ray free electron lasers (XFELs) [22], [23], [24], [25], [26], high harmonic generation [27], [28], [29], [30], soft X-ray laser [31], optical laser [32], and electrons [33], [34], [35]. Several readable reviews on the development and implementation of phase-retrieval algorithms for the specific application of CDI were written by Marchesini [11], Thibault and Elser [36] and Nugent [37]. Presently, one of the most challenging problems in CDI is towards 3D structural determination of large protein molecules [7], [38]. There has been ongoing progress towards this goal during the past decade. In 2006, Chapman et al., demonstrated the CDI of a test sample using intense ultra-short single pulse from free electron laser, relying on recording a diffraction pattern before the sample was destroyed [24]. Recently, the technique was implemented for high-resolution imaging of isolated sub-micron objects, such as herpesvirus [39], mimivirus [25] and aerosol particles such as soot [26].

From a theoretical and algorithm perspective, phase retrieval is a difficult problem, in many cases lacking a unique solution. Furthermore, even with the existence of a unique solution, there is not necessarily a guarantee that it can be found algorithmically. Nevertheless, as reasoned above, phase retrieval algorithms and applications have benefited from a surge of research in recent years, in large part due to various new imaging techniques in optics. This trend has begun impacting the signal processing community as well – the past few years have witnessed growing interest within this community in developing new approaches to phase retrieval by using tools of modern optimization theory [41], [42]. More recent work has begun exploring connections between phase retrieval and structure-based information processing [43], [44], [45], [46], [47], [48]. For example, it has been shown that, by exploiting the sparsity of many optical images, one can develop powerful phase retrieval methods that allow for increased resolution considerably beyond Abbe's diffraction limit, resolving features smaller than $1/5$ of the wavelength [48]. The relationship between the fields of sparsity and optical imaging has led to an important generalization of the basic principles of sparsity-based reconstruction to nonlinear measurement systems [44], [49], [47], [50], [51], [52], [53], [54], [55], [56]. Here too, optics played an important role in signal processing: since the phase retrieval problem is inherently mathematically nonlinear (i.e., the sought signal is related to the measurements nonlinearly), employing sparsity-based concepts in phase retrieval required genuine modifications to the linear sparsity-based algorithms known from the field of compressed sensing [57]. We believe that this field will grow steadily in the next few years, with rapid development of coherent X-ray sources worldwide [58], [59] and more researchers contributing to the theory, algorithms and practice of nonlinear sparse recovery.

III. MATHEMATICAL FORMULATION

A. Problem Formulation

Consider the discretized 1D real space distribution function of an object: $\mathbf{x} \in \mathbb{C}^N$ (extension of the formulation to higher dimensions is trivial). In CDI, for example, this corresponds to the transmittance function of the object. The fact that $\mathbf{x}$ is in general complex, corresponds physically to the fact that the electromagnetic field emanating from different points on the

Coherent Diffractive Imaging (CDI)

In the basic CDI setup (forward scattering), an object is illuminated by a quasi-monochromatic coherent wave, and the diffracted intensity is measured (Fig. 2). When the object is small and the intensity is measured far away, the measured intensity is proportional to the magnitude of the Fourier transform of the wave at the object plane, with appropriate spatial scaling.
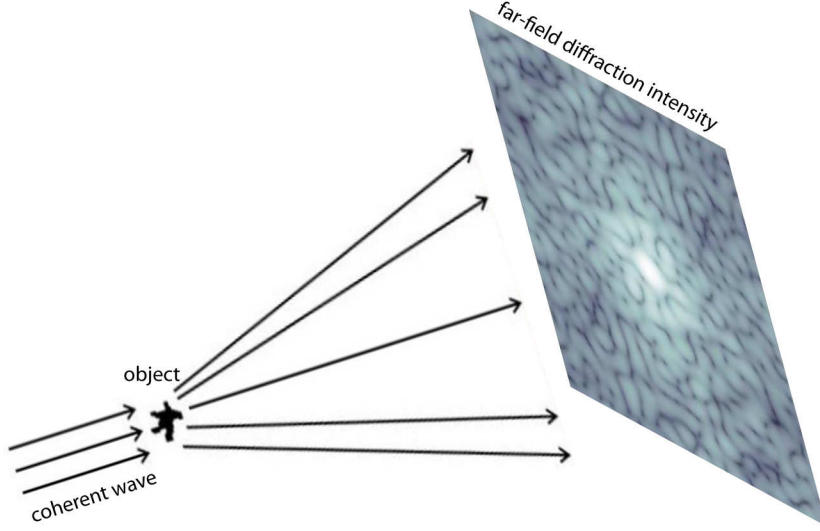

Figure 2. A forward-scattering CDI setup: A coherent wave diffracts from an object (the *sought information*), and produces a far-field intensity pattern corresponding to the magnitude of the Fourier transform of the object.

In optics terms, when the Fresnel number is small ($N_F = \frac{a^2}{\lambda d} << 1$, where a is a radius confining the object in the object plane, d is the distance between the object and the measured intensity plane, and λ is the wavelength of the light), the relation between the measured intensity I_{out} and the wave at the object plane E_{in}, is given by [40]:

$$I_{out}(x,y) \propto \left| \hat{E}_{in} \left(\frac{x}{\lambda d}, \frac{y}{\lambda d} \right) \right|^2$$

with $\hat{E}_{in} = \mathcal{F}\{E_{in}\}$, and $\mathcal{F}$ denoting the Fourier transform. Once the far field intensity is measured, the goal is to recover E_{in} (which is equivalent to recovering the object) from I_{out}. This requires solving the phase retrieval problem, which is attempted using an algorithm such as the ones described in this review paper.

object has not only magnitude but also phase (as is always the case, for example, when 3D objects are illuminated and light is reflected from point at different planes). The 1D discrete Fourier transform (DFT) of $\mathbf{x}$ is given by:

$$X[k] = \sum_{n=0}^{N-1} x[n]e^{-j2\pi \frac{kn}{N}}, \quad k = 0, 1, ..., N-1. \quad (1)$$

The term *oversampled DFT* used in this paper will refer to an M point DFT of $\mathbf{x} \in \mathbb{C}^N$ with $M > N$:

$$X[k] = \sum_{n=0}^{N-1} x[n]e^{-j2\pi \frac{kn}{M}}, \quad k = 0, 1, \dots, M-1. \quad (2)$$

Recovery of $\mathbf{x}$ from measurement of $\mathbf{X}$ can be achieved by simply applying the inverse-DFT operator. Writing $X[k] = |X[k]| \cdot e^{j\phi[k]}$, the Fourier phase retrieval problem is to recover $\mathbf{x}$ when only the magnitude of X is measured, i.e. to recover $x[n]$ given $|X[k]|$. Since the DFT operator is bijective, this is equivalent to recovering the phase of $X[k]$, namely, $\phi[k]$

- hence the name *phase retrieval*. Denote by $\hat{\mathbf{x}}$ the vector $\mathbf{x}$ after padding with $N-1$ zeros. The autocorrelation sequence of $\hat{\mathbf{x}}$ is then defined as:

$$g[m] = \sum_{i=\max\{1,m+1\}}^{N} \hat{x}_i \overline{\hat{x}_{i-m}}, \quad m = -(N-1), \dots, N-1. \quad (3)$$

It is well known that the DFT of $g[m]$, denoted by $G[k]$, satisfies $G[k] = |X[k]|^2$. Thus, the problem of recovering a signal from its Fourier magnitude is equivalent to the problem of recovering a signal from the autocorrelation sequence of its oversampled version.

Continuous phase retrieval can be defined similarly to its discrete counterpart, as the recovery of a 1D signal $f(x)$ from its continuous Fourier magnitude:

$$|F(\nu)| = \left| \int_{\mathbb{R}} f(x) \exp(-j2\pi\nu x)dx \right|.$$

The actual objects of interest, electromagnetic fields, are

usually described by continuous functions. However, since the data acquisition is digitized (by CCD camera and alike), and the processing is done digitally, we shall mostly treat here the discrete case.

The Fourier phase retrieval problem is as a special case of the more general phase retrieval problem, where we are given measurements:

$$y_k = |\langle \mathbf{a}_k, \mathbf{x} \rangle|^2, \quad k = 1, \ldots, M, \qquad (4)$$

with $\mathbf{a}_k$ denoting the measurement vectors. In discrete 1D Fourier phase retrieval the measurement vectors are given by $\mathbf{a}_k[n] = e^{-j2\pi \frac{kn}{M}}$. For mathematical analysis, it is often easier to treat the case where the measurements are random (i.e. $\mathbf{a}_k$ are random vectors), as this allows uniqueness guarantees that are otherwise hard to obtain [60], [41], [53], [61], [62]. Nevertheless, more structured measurements have also been investigated [63].

Before proceeding to the mathematical methodology, it is important to highlight the significance of knowing the Fourier phase. In fact, it is well known that knowledge of the Fourier phase is crucial in recovering an object from its Fourier transform [64]. Many times the Fourier phase contains more information than the Fourier magnitude, as can be seen in the synthetic example shown in Fig. 3. The figure shows the result of the following numerical experiment: Two images (Cameraman and Lenna) are Fourier transformed. The phases of their transforms are swapped, and subsequently they are inverse Fourier transformed. It is evident, for this quite arbitrary example, that the Fourier phase contains a significant amount of information about the images. In crystallography, this phenomenon is the source of genuine concern of *phase bias* of molecular models (such as used in molecular replacement) in refined structures.

In the remainder of this section we discuss uniqueness of the phase retrieval problem, i.e. under what conditions is the solution to the phase problem unique? It is worth noting that, while the discussion of theoretical uniqueness guarantees is important and interesting, the lack of such guarantees does not prevent practical applications from producing excellent reconstruction results in many settings.

B. Uniqueness

1) Fourier measurements: The recovery of a signal from its Fourier magnitude alone, in general, does not yield a unique solution. This section will review the main existing theoretical results regarding phase-retrieval uniqueness.

First, there are so called *trivial* ambiguities that are always present. The following three transformations (or any combination of them) conserve Fourier magnitude:

1. Global phase shift: $x[n] \Rightarrow x[n] \cdot e^{j\phi_0}$
2. Conjugate inversion: $x[n] \Rightarrow \overline{x[-n]}$
3. Spatial shift: $x[n] \Rightarrow x[n + n_0]$.

Second, there are non-trivial ambiguities, the situation of which varies for different problem-dimensions. In the 1D problem there is no uniqueness – i.e. there are multiple 1D signals with the same Fourier magnitude. Even if the support of the signal is bounded within a known range, uniqueness does not exist [65]. Any pair of 1D signals having the same autocorrelation function yields the same Fourier magnitude, as the two are connected by a Fourier transform. Consider for example the two vectors $\mathbf{u} = [1\ 0\ -2\ 0\ -2]^T$ and $\mathbf{v} = [(1 - \sqrt{3})\ 0\ 1\ 0\ (1 + \sqrt{3})]^T$. Both of these vectors have the same support, and yield the same autocorrelation function $g[m] = [-2, 0, 2, 0, 9, 0, 2, 0, -2]$. Therefore, they are indistinguishable by their Fourier magnitude, even though they are not *trivially* equivalent.

For higher dimensions (2D and above), Bruck and Sodin [66], Hayes [67], and Bates [68] have shown that, with the exception of a set of signals of measure zero, a real $d \geq 2$ dimensional signal with support $\mathbf{N} = [N_1 \ldots N_d]$, namely $x(n_1, \ldots, n_d) = 0$ whenever $n_k < 0$ or $n_k \geq N_k$ for $k = 1, \ldots, d$ is uniquely specified by the magnitude of its continuous Fourier transform, up to the trivial ambiguities mentioned above. Furthermore, the magnitude of the oversampled $\mathbf{M}$ point DFT sequence of the signal, with $\mathbf{M} \geq 2\mathbf{N} - 1$ (where the inequality holds in every dimension), is sufficient to guarantee uniqueness. The problematic set of signals that are not uniquely defined by their Fourier magnitudes are those having a reducible $\mathbf{Z}$ transform: denoting the d dimensional Z transform of x by $X(z_1, \ldots, z_d) = \sum_{n_1} \cdots \sum_{n_d} x(n_1, \ldots, n_d) z_1^{-n_1} \cdots z_d^{-n_d}$, $X(\mathbf{z})$ is said to be reducible if it can be written as $X(\mathbf{z}) = X_1(\mathbf{z})X_2(\mathbf{z})$, where $X_1(\mathbf{z})$ and $X_2(\mathbf{z})$ are both polynomials in $\mathbf{z}$ with degree $p > 0$. It is important to note that in practice, for typical images, a number of samples smaller than $2\mathbf{N} - 1$ is many times sufficient (even $\mathbf{M} = \mathbf{N}$ can work [69]), however the exact guarantees relating the number of samples to the type of images remains an open question.

Additional prior information about the sought signal, other than its support, can be incorporated, and will naturally improve the conditioning of the problem. For example, knowledge of the Fourier phase sign (i.e. 1 bit of phase information)
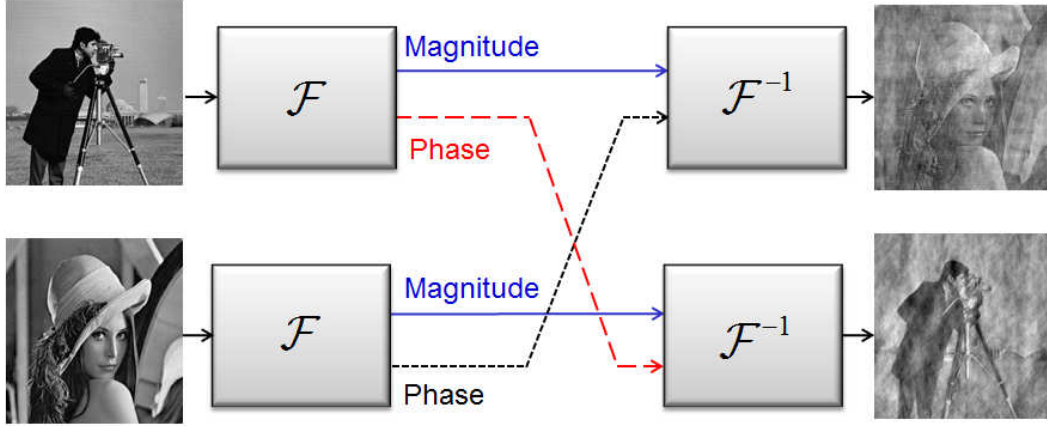
Figure 3.   The importance of Fourier phase. Two images, Cameraman and Lenna, are Fourier transformed. After swapping their phases, they are inverse Fourier transformed. The result clearly demonstrates the importance of phase information for image recovery.

has been shown [70] to yield uniqueness with some restrictions on the signal (specifically that the signal is real and its Z transform has no zeros on the unit circle). A different, popular type of prior knowledge that has been used recently in various applications [57], [71], is that the signal $\mathbf{x} \in \mathbb{C}^N$ is sparse - i.e. contains only a small number k of nonzero elements, with $k \ll N$. The exact locations and values of the nonzero elements are not known a-priori. In this case, it has been shown [72] that knowledge of the full autocorrelation sequence of a 1D k sparse real signal $\mathbf{x}$ is sufficient in order to uniquely define $\mathbf{x}$, as long as $k \neq 6$ and the autocorrelation sequence is *collision free*. A vector $\mathbf{x}$ is said to have a collision free autocorrelation sequence if $x(i) - x(j) \neq x(k) - x(l)$, for all distinct $i, j, k, l \in \{1, \ldots N\}$ that are the locations of distinct nonzero values in $\mathbf{x}$. In addition, under these conditions, only M Fourier magnitude measurements are sufficient to uniquely define the autocorrelation sequence and therefore the signal $\mathbf{x}$, as long as M is prime and $M \geq k^2 - k + 1$ [73]. An interesting perspective relating phase retrieval to the Turnpike problem, namely, reconstructing a set of integers from their pairwise distances, is presented in [74].Using this approach, the authors prove uniqueness with high probability, for random signals having a non-periodic support.

2) General measurements: Considering inner products with general, non-Fourier (typically - random) measurement vectors, allows simpler derivation of theoretical guarantees. There have been several theoretical results relating the number and the nature of the measurements that are required for uniqueness, mostly dealing with random measurement vectors. The work of Balan [43] implies that for real signals in $\mathbb{R}^N$, $2N-1$ random measurements are needed, provided that they are full-

spark, i.e. that every subset of N measurement vectors spans $\mathbb{R}^N$ [46]. This result was later extended to the complex case [46], where it is conjectured that $4N - 4$ *generic* measurements, as defined in [46], are sufficient for bijectivity. In terms of stability, i.e. when the measurements are noisy, it has been proven [53] that on the order of $N \log(N)$ measurements (or $k \log(N)$ measurements in the k sparse case) are sufficient for stable uniqueness. It was also shown that minimizing the (nonconvex) least-squares objective: $\sum |y_i^2 - |\langle \mathbf{a}_i, \mathbf{x} \rangle|^2|^p$, with $1 < p \leq 2$, yields the correct solution under these conditions [53]. For the noiseless case, any k-sparse vector in $\mathbb{R}^N$ has been shown to be uniquely determined by $4k - 1$ random Gaussian intensity measurements with high probability [73].

To study the injectivity of general (i.e. not necessarily random) measurements, the *complement-property* has been introduced in [43] for the real case. An extension was presented in [46] for the complex setting. A set of measurement vectors $\{\mathbf{a}_i\}_{i=1}^M$ with $a_i \in \mathbb{R}^N$ satisfies the complement property if for every $S \subseteq \{1, \ldots, M\}$, either $\{\mathbf{a}_i\}_{i \in S}$ or $\{\mathbf{a}_i\}_{i \in S^C}$ span $\mathbb{R}^N$. It has been shown in [43] that the mapping constructed by $y_i = |\langle \mathbf{a}_i, \mathbf{x} \rangle|$, $i = 1, \ldots, N$ is injective if and only if the measurement set satisfies the complement property. This poses a lower limit on the number of necessary measurements $M > 2N - 1$.

The results reviewed in this section are summarized in Table I. In addition, there is a large amount of work on phase retrieval uniqueness under different conditions, e.g. when the phase is known only approximately [75], or from redundant masked Fourier measurements [76], [45].

Fourier measurements	1D	No uniqueness [Hofstetter 1964]
	≥2D	Uniqueness for real non-reducible signals. Requires oversampling by ≈2 [Hayes 1982]
	k-sparse 1D	Uniqueness for signals with collision free autocorrelation (and $k \neq 6$) [Ranieri 2013] M Fourier magnitude measurements are sufficient, for a prime $M \geq k^2 - k + 1$ [Ohlsson 2013]
General measurements	Real signal R^N	Satisfying the Complement-property is necessary and sufficient. $2N - 1$ full-spark random measurements guarantee uniqueness w.h.p. [Balan 2006]
	Real signal R^N (Noisy)	$N \log(N)$ measurements (or $k \log(N)$ measurements in the k-sparse case) are sufficient for stable uniqueness [Eldar 2012]
	Complex signal C^N	Conjecture: $4N - 4$ generic measurements are sufficient [Bandeira 2013]

Table I
PHASE RETRIEVAL - UNIQUENESS

IV. ALGORITHMS

Despite the uniqueness guarantees, no known general solution method exists to actually find the unknown signal from its Fourier magnitude given the other constraints. Over the years, several approaches have been suggested for solving the phase retrieval problem, with the popular ones being alternating projection algorithms [77], [2], [78]. In addition, methods were suggested attempting to solve phase retrieval problems by using exposures with different masks [76], or images obtained at different propagation planes [79], [80]. Another method to obtain additional information is scanning CDI, (also termed ptychography) [81], [82], [20], which uses several different illumination patterns to obtain coherent diffraction images.

In this section we survey existing phase retrieval algorithms, including general algorithms (sub-Section IV-A), and sparsity based algorithms, i.e. algorithms exploiting prior knowledge in the form of signal-sparsity (sub-Section IV-B).

A. General algorithms

The general phase retrieval problem we wish to solve can be formulated as the following least squares problem, or empirical risk minimization:

$$\min_{\mathbf{x}} \sum_{k=1}^{M} \left(y_k - |\langle \mathbf{a}_k, \mathbf{x} \rangle|^2 \right)^2, \tag{5}$$

with $\mathbf{y}$ being the measurements and $\mathbf{a}_k$ being the measurement vectors defined in (4). In general we can replace the square in the objective by any power p. Unfortunately, this is a non-

convex problem, and it is not clear how to find a global minimum even if one exists. In this section we describe several approaches that have been suggested to deal with this problem, and types of prior information that can be incorporated into these methods in order to increase the probability of convergence to the true solution.

1) Alternating projections: The most popular class of phase retrieval methods is based on alternate projections. These methods were pioneered by the work of Gerchberg and Saxton [77], dealing with the closely related problem of recovering a complex image from magnitude measurements at two different planes - the real (*imaging*) plane and Fourier (*diffraction*) plane. The original Gerchberg-Saxton (GS) algorithm consists of iteratively imposing the real-plane and Fourier-plane constraints, namely, the measured real-space magnitude $|x[n]|$ and Fourier magnitude $|X[k]|$, as illustrated in Fig. 4a. The GS algorithm is described in Algorithm 1. The recovery error, defined as $E_i = \sum_k \left| |Z_i[k]| - |X[k]| \right|^2$ is easily shown to be monotonically decreasing with i [78]. Despite this fact, recovery to the true solution is not guaranteed, as the algorithm can converge to a local minimum.

Extending the GS projection ideas further, Fienup in 1978 [2] suggested a modified version of the GS algorithm, in which the real-space magnitude constraints may be replaced by other types of constraints, in addition to consistency with the measured Fourier magnitude. The real-space constraints may be for example non-negativity, a known signal support, namely $x[i] = 0$ for all $i > N_0$, where N_0 is known (or approximately
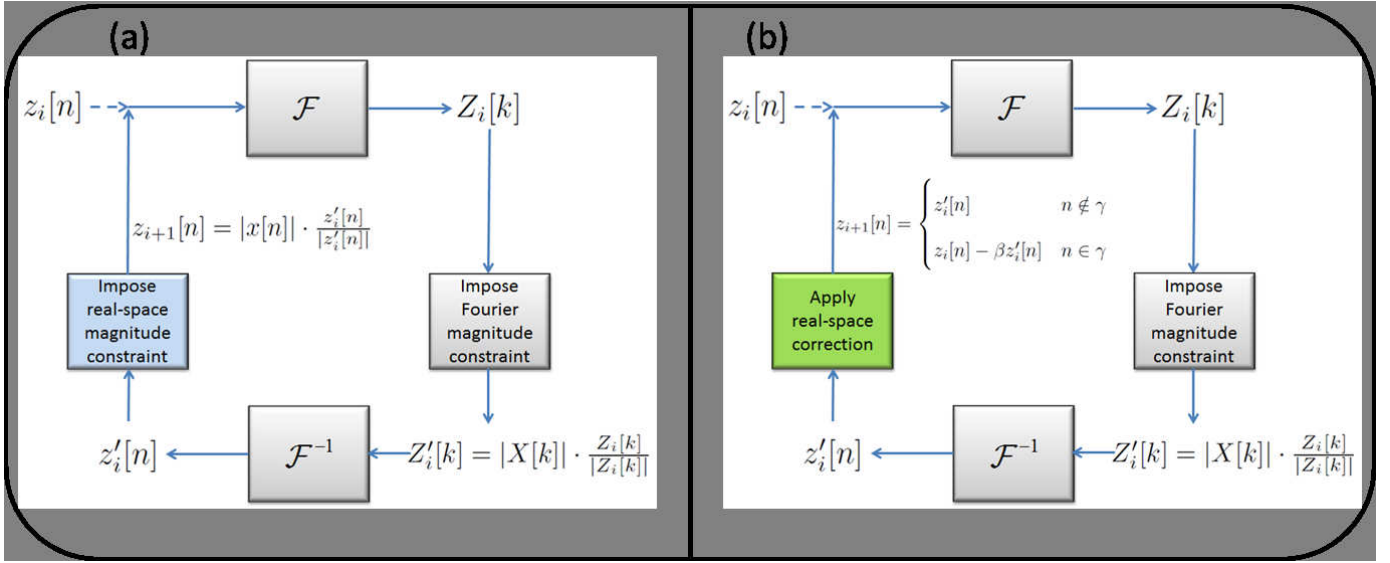
Figure 4. (a) Block diagram of the Gerchberg-Saxton algorithm. (b) Block diagram of the Fienup HIO algorithm. The algorithms differ in their fourth (colored) step.

Algorithm 1 Gerchberg-Saxton (GS)

Input: $|x[n]|, |X[k]|, \epsilon$
$|x[n]|$ - Real space magnitude
$|X[k]|$ - Fourier magnitude
ϵ - Error threshold
Output: $z[n]$ - a vector that conforms with both magnitude constraints, i.e.: $|z[n]| = |x[n]|$, and $|Z[k]| = |X[k]|$, where $Z[k]$ is the DFT of $z[n]$

Initialization. Choose initial $z_0[n] = |x[n]| \exp(\phi[n])$ (e.g. with a random $\phi[n]$).
General Step ($i = 1, 2, \ldots$)**:**
  1) Fourier transform $z_i[n]$ to obtain $Z_i[k]$
  2) Keep current Fourier phase, but impose Fourier magnitude constraint: $Z_i'[k] = |X[k]| \cdot \frac{Z_i[k]}{|Z_i[k]|}$
  3) Inverse Fourier transform $Z_i'[k]$ to obtain $z_i'[n]$
  4) Keep current real-space phase, but impose real-space magnitude constraint: $z_{i+1}[n] = |x[n]| \cdot \frac{z_i'[n]}{|z_i'[n]|}$
  5) Go to 1
Until $E_i = \sum_k \left| |Z_i[k]| - |X[k]| \right|^2 \le \epsilon$

---

known), or both. The basic framework of the Fienup methods is similar to GS - in fact, the first three steps are identical. Step 4), however, replaces imposing the real-space magnitude constraint by applying a correction to the real-space estimate. Some possible variants to this step were also suggested [78]. Here we describe the one most commonly used, referred to as the hybrid-input output (HIO) method, which consists of the following correction step:

  4) Obtain $z_{i+1}[n]$ by applying a correction to the real-space

image estimate:

$$z_{i+1}[n] = \begin{cases} z_i'[n], & n \notin \gamma \\ z_i[n] - \beta z_i'[n], & n \in \gamma, \end{cases} \quad (6)$$

with β being a small parameter, and γ being the set of indices for which $z_i'[n]$ violates the real-space constraints.

The real-space constraint violation may be a support violation (signal is nonzero where it should be zero), or a non-negativity violation.

The Fienup algorithm is represented schematically in Fig. 4b. There is no proof that the HIO algorithm converges. It is also known to be sensitive to the accuracy of the prior information (e.g. the real-space support needs to be tightly known, especially in the complex signal case [83]). Nonetheless, in practice, the simple HIO based methods are commonly used in optical phase retrieval applications such as CDI [84], [85], [86]. Other variants of the correction step include the Input-Output method, and the Output-Output method [78], corresponding respectively to

$$z_{i+1}[n] = \begin{cases} z_i[n], & n \notin \gamma \\ z_i[n] - \beta z_i'[n], & n \in \gamma, \end{cases}$$
$$z_{i+1}[n] = \begin{cases} z_i'[n], & n \notin \gamma \\ z_i'[n] - \beta z_i'[n], & n \in \gamma. \end{cases} \quad (7)$$

An important feature of the HIO algorithm is its empirical ability to avoid local minima and converge to a global minimum for noise-free oversampled diffraction patterns. However,

when there is high noise present in the diffraction intensity, HIO suffers from several limitations. First, the algorithm sometimes becomes stagnant and fails to converge to a global minimum. Second, a support has to be pre-defined. Third, the image oscillates as a function of the iteration. Over the years, various algorithms have been developed to overcome these limitations, including the combination of HIO and the error-reduction (ER) algorithm [78], difference map [10], hybrid projection reflection [12], guided hybrid input-output (GHIO) [87], relaxed averaged alternating reflectors (RAAR) [13], noise robust (NR)-HIO [88], and oversampling smoothness (OSS) [14]. An analysis of iterative phase retrieval algorithms from a convex optimization perspective can be found in [89].

As an exapmle, the recently proposed OSS algorithm exhibits improved performance over HIO and its variants in many settings. OSS is based on Fienup iterations, with an added smoothing Gaussian filter applied to the off-support region in the real space object in each iteration. Namely, the fourth step in HIO is replaced by:

$$z''[n] = \begin{cases} z_i'[n], & n \notin \gamma \\ z_i[n] - \beta z_i'[n], & n \in \gamma, \end{cases}$$
$$z_{i+1}[n] = \begin{cases} z_i''[n], & n \notin \gamma \\ \mathcal{F}\{Z_i''[k]W[k]\}, & n \in \gamma, \end{cases} \quad (8)$$

where $W[k]$ is a Gaussian function, with its variance decreasing with iterations. A quantitative comparison for a specific example between OSS and HIO can be found in Section V-A. For a comparison and numerical investigation of several alternate projection algorithms see for example [11], [14].

As performance of the Fienup methods is dependent on the initial points, it is possible and recommended to try several initializations. In [61], the authors consider a clever method for initial point selection, and show that for the random Gaussian measurement case, the resulting iterations yield a solution arbitrarily close to the true vector.

2) Semi-Definite Programming (SDP) based algorithms: An alternative recently developed to solve the phase retrieval problem is based on semidefinite relaxation [90], [49], [42]. The method relies on the observation that (4) describes a set of quadratic equations, which can be re-written as linear equations in a higher dimension. Specifically, define the $N \times N$ matrix $\mathbf{X} = \mathbf{x}\mathbf{x}^*$. The measurements (4) are then linear in $\mathbf{X}$:

$$y_k = |\langle \mathbf{a}_k, \mathbf{x} \rangle|^2 = \mathbf{x}^* \mathbf{a}_k \mathbf{a}_k^* \mathbf{x} = \mathbf{x}^* \mathbf{A}_k \mathbf{x} = \text{Tr}(\mathbf{A}_k \mathbf{X}), \quad (9)$$

where $\mathbf{A}_k = \mathbf{a}_k \mathbf{a}_k^*$. Our problem is then to find a matrix $\mathbf{X} = \mathbf{x}\mathbf{x}^*$ that satisfies (9). The constraint $\mathbf{X} = \mathbf{x}\mathbf{x}^*$ is equivalent to the requirement that $\mathbf{X}$ has rank one, and is positive semi-definite, which we denote by $\mathbf{X} \succeq 0$. Therefore, finding a vector $\mathbf{x}$ satisfying (4) can be formulated as:

$$\begin{aligned} \text{find} \quad & \mathbf{X} \\ \text{s.t.} \quad & y_k = \text{Tr}(\mathbf{A}_k \mathbf{X}), \quad k = 1, \dots, M, \\ & \mathbf{X} \succeq 0, \\ & \text{rank}(\mathbf{X}) = 1. \end{aligned} \quad (10)$$

Problem (10) is equivalent to the following rank minimization problem:

$$\begin{aligned} \text{min} \quad & \text{rank}(\mathbf{X}) \\ \text{s.t.} \quad & y_k = \text{Tr}(\mathbf{A}_k \mathbf{X}), \quad k = 1, \dots, M, \\ & \mathbf{X} \succeq 0. \end{aligned} \quad (11)$$

Unfortunately, rank minimization is a hard combinatorial problem. However, since the constraints in (11) are convex (in fact linear), one might try to relax the minimum rank objective, for example by replacing it with minimization of $\text{Tr}(\mathbf{X})$. This approach is referred to as PhaseLift [42]. Alternatively, one may use the log-det reweighted rank minimization heuristic suggested in [91], which is the approach followed in [49], [41]. In [41] it is shown that PhaseLift yields the true vector $\mathbf{x}$ with large probability, when the measurements are random Gaussian and $M \sim O(N \log N)$.

The SDP approach requires matrix lifting, namely, replacing the sought vector with a higher dimensional matrix, followed by solving a higher dimensional problem. It is therefore, in principle, more computationally demanding than the alternating projection approaches, or greedy methods, which will be discussed in the next section. In addition, in general there is neither a guarantee that the rank minimization process will yield a rank-one matrix, nor that the true solution is found, even if there is a unique solution.

B. Sparsity based algorithms

A specific kind of prior knowledge that can be incorporated into the phase retrieval problem to help regularize it, is the fact that the sought real-space object is sparse in some known representation (See sparse linear problems box). This means that the object $\mathbf{x}$ can be written as:

$$\mathbf{x} = \mathbf{\Psi}\boldsymbol{\alpha} \quad (12)$$

with $\mathbf{\Psi}$ being a representation matrix (the sparsity basis), and $\boldsymbol{\alpha}$ being a sparse vector, i.e. a vector containing a small number

of nonzero coefficients. The simplest example is when the object is composed of a small number of point sources (in which case $\mathbf{\Psi}$ is the identity matrix). Armed with such prior knowledge, one can hope to improve the performance of phase retrieval algorithms, by limiting the search for the true vector to the set of sparse vectors. There are several different ways that such knowledge can be incorporated, which are described in this subsection.

Alternating projections with sparsity prior: The Fienup algorithm, described in Section IV-A1, allows in principle incorporation of various types of general knowledge about the object, including sparsity [44], [92]. The method in [92], for example, is based on the Fienup iterations, with the first three steps remaining unchanged. Step 4, is replaced by projection and thresholding. Assuming an invertible $\mathbf{\Psi}$ and a k sparse vector $\boldsymbol{\alpha}$ such that $\mathbf{x} = \mathbf{\Psi}\boldsymbol{\alpha}$:

4) Obtain $z_{i+1}[n]$ by projecting $z_i'[n]$ onto $\mathbf{\Psi}$, thresholding, and projecting back. Namely:

   a) Calculate $\boldsymbol{\alpha}_i = \mathbf{\Psi}^{-1}\mathbf{z}_i'$
   b) Keep only the k largest elements of $|\mathbf{a}_i|$, setting the rest to zero.
   c) Set $\mathbf{z}_{i+1} = \mathbf{\Psi}\boldsymbol{\alpha}_i$.

Similarly to the GS method, the error here can be shown to be nonincreasing, so that convergence to a local minimum is guaranteed [92].

Note, that while this method is suggested in [92] for an orthonormal basis $\mathbf{\Psi}$, it can be easily modified to accommodate a non-invertible $\mathbf{\Psi}$. This can be done by replacing parts (a)+(b) with finding a sparse solution $\mathbf{a}_i$ to $\mathbf{z}_i = \mathbf{\Psi}\mathbf{a}_i$, using any sparse solution method [57].

SDP based methods with sparsity prior: SDP based methods can also be modified to account for prior knowledge of signal sparsity. The incorporation of sparsity can be performed in several different ways. The first work to suggest sparsity-based SDP phase-retrieval came from the domain of optics, and dealt with partially spatially-incoherent illumination [49]. This work actually considered a theoretical problem of greater complexity, combining phase retrieval with sub-wavelength imaging. Experimental results on sub-wavelength CDI can be found in [48], where the sought signal is an actual optical image with subwavelength features, and the measured data corresponds to the Fourier magnitude sampled by a camera at the focal plane of a microscope lens.

The method suggested in [49], dubbed QCS for Quadratic Compressed Sensing, is based on adding sparsity constraints to the rank minimization problem (11). When $\mathbf{x}$ is sparse, the result of the outer product $\mathbf{X} = \mathbf{x}\mathbf{x}^*$ is a sparse matrix as well, as shown in Fig. 5. Therefore, one strategy might be to minimize the l_1 norm of the matrix $\mathbf{X}$. Alternatively, it is possible to exploit further the structure of $\mathbf{X}$, by noticing that the number of rows in $\mathbf{X}$ with a nonzero norm is equal to the number of non-zero values in $\mathbf{x}$. This means that sparsity of $\mathbf{x}$ also implies a small number of non-zero rows in $\mathbf{X}$. Consider the vector $\mathbf{p}$ containing the l_2 norm of the rows of $\mathbf{X}$, i.e. $p_j = \left(\sum_k |X_{jk}|^2 \right)^{\frac{1}{2}}$ (note that the l_2 norm can be replaced by any other norm). Since $\mathbf{p}$ should be sparse, one might try to impose a low l_1 norm on $\mathbf{p}$, in the spirit of l_1 minimization for the sparse linear problem. This yields the constraint $||\mathbf{p}||_1 = \sum_j |p_j| = \sum_j \left(\sum_k |X_{jk}|^2 \right)^{\frac{1}{2}} \leq \eta$, corresponding exactly to a low mixed l_{1-2} norm constraint on $\mathbf{X}$ [99]. The problem to solve, as cast in [49] is therefore :

$$
\begin{aligned}
\min \quad & \text{rank}(\mathbf{X}) \\
\text{s.t.} \quad & |\text{Tr}(\mathbf{A}_k\mathbf{X}) - y_k| \leq \epsilon, \quad k = 1, \ldots, M, \\
& \mathbf{X} \succeq 0, \\
& \sum_j \left(\sum_k |X_{jk}|^2 \right)^{\frac{1}{2}} \leq \eta,
\end{aligned}
\tag{19}
$$

where ϵ is a noise parameter, and η is a sparsity parameter, enforcing row sparsity of $\mathbf{X}$.

Since finding a rank 1 matrix $\mathbf{X}$ satisfying the constraints is NP hard, the solution to (19) is approximated in ([49]) using the iterative log-det heuristic proposed in [91], with an additional thresholding step added at each iteration, to further induce signal sparsity. Once a low rank matrix $\hat{\mathbf{X}}$ that is consistent with the measurements and the sparse priors is found, the sought vector $\mathbf{x}$ is estimated by taking the best rank 1 approximation of $\hat{\mathbf{X}}$ using the singular value decomposition (SVD): Decomposing $\hat{\mathbf{X}}$ into $\hat{\mathbf{X}} = \mathbf{U}\mathbf{S}\mathbf{V}^\mathbf{T}$, the rank-1 approximation of $\hat{\mathbf{X}}$ is taken as $\hat{\mathbf{X}}_\mathbf{1} = S_{11}\mathbf{U}_\mathbf{1}\mathbf{U}_\mathbf{1}^*$, where S_{11} represents the largest singular value, and $\mathbf{U}_\mathbf{1}$ is the corresponding column of $\mathbf{U}$.

Similar ideas that add sparse priors to SDP methods have been later suggested in [50], [100], [60]. In [50], the rank minimization objective is relaxed to a convex trace minimization, with an additional l_1 regularization term to induce sparsity. This formulation yields:

$$
\begin{aligned}
\min \quad & \text{Tr}(\mathbf{X}) + \lambda||\mathbf{X}||_1 \\
\text{s.t.} \quad & |\text{Tr}(\mathbf{A}_k\mathbf{X}) - y_k| \leq \epsilon \quad k = 1, \ldots, M, \\
& \mathbf{X} \succeq 0.
\end{aligned}
\tag{20}
$$

The solution of (20) is shown [50] to be unique in the noiseless

---

Sparse Linear Problems

Finding sparse solutions to sets of equations is a topic that has drawn much attention in recent years [93], [94], [57], [71]. Consider the linear system:

$$\mathbf{y} = \mathbf{A}\mathbf{x} \tag{13}$$

with $\mathbf{y}$ being a set of M linear measurements, $\mathbf{A}$ being an $M \times N$ measurement matrix, and $\mathbf{x}$ being the unknown length-N vector. When the system is underdetermined (i.e. $M < N$), there are infinitely many possible solutions $\mathbf{x}$. A key result of the theory of sparse recovery is that adding the constraint that $\mathbf{x}$ is sparse, i.e. contains only a few nonzero entries guarantees a unique solution to (13), under general conditions for $\mathbf{A}$. One such condition is based on the *coherence* of $\mathbf{A}$ [95]:

$$||\mathbf{x}||_0 \leq \frac{1}{2}\left(1 + \frac{1}{\mu}\right) \tag{14}$$

with $||\mathbf{x}||_0$ being the number of nonzero entries in $\mathbf{x}$, and the coherence defined by:

$$\mu = \max_{i,j} \frac{< \mathbf{A}_i, \mathbf{A}_j >}{||\mathbf{A}_i|| \cdot ||\mathbf{A}_j||}. \tag{15}$$

Here, we denote by $\mathbf{A}_i$ the ith column of $\mathbf{A}$, and by $||\mathbf{A}_i||$ its Euclidean norm.
Under (14), one can find the unique solution to (13) by solving

$$\min_{\mathbf{x}} ||\mathbf{x}||_0 \quad \text{s.t.} \quad \mathbf{y} = \mathbf{A}\mathbf{x}. \tag{16}$$

Unfortunately, (16) is an NP-hard combinatorial problem. However, many methods have been develop to approximately solve (16). One class of such methods consists of greedy algorithms such as Orthogonal Matching Pursuit [96]. Another popular method is based on convex relaxation of the l_0 norm to an l_1 norm [97], which yields the convex problem:

$$\min_{\mathbf{x}} ||\mathbf{x}||_1 \quad \text{s.t.} \quad \mathbf{y} = \mathbf{A}\mathbf{x}. \tag{17}$$

In fact, under the condition (14), it has been shown [95] that the solution to (17) is equal to the solution of (16).

Another important criterion to evaluate the recovery ability in sparse linear problems of the form (13) is the restricted isometry property (RIP) [98] of $\mathbf{A}$, defined as follows: For an an $M \times N$ matrix $\mathbf{A}$ (with $M < N$), define δ_k as the smallest value such that for every submatrix $\mathbf{A}_k$ composed of k columns of $\mathbf{A}$, it holds that

$$(1 - \delta_k)||\mathbf{x}||_2^2 \leq ||\mathbf{A}_k\mathbf{x}||_2^2 \leq (1 + \delta_k)||\mathbf{x}||_2^2, \quad \forall \mathbf{x} \in \mathbb{R}^k. \tag{18}$$

The RIP is therefore a measure of whether $\mathbf{A}$ preserves the energy of any k sparse signal - which is the case if δ_k is small. In the context of sparse recovery, it is used to prove uniqueness and noise-robustness results. For example, if $\mathbf{A}$ is such that $\delta_{2k} < \sqrt{2} - 1$, then solving (17) will yield the unique sparse solution to (13). In practice, it is combinatorially difficult to calculate the RIP of a given matrix. However, certain random matrices can be shown to have 'good RIP' with high probability. For example, an $M \times N$ iid Gaussian matrix obeys the k-RIP with high probability, for $M \sim O(k \log(N/k))$ [93]. This is one of the reasons that random matrices are favorable for sparse sensing.

---

case ($\epsilon = 0$), under the following condition: $||\bar{\mathbf{X}}||_0 \leq \frac{1}{2}\left(1 + \frac{1}{\mu}\right)$, where $\bar{\mathbf{X}} = \bar{\mathbf{x}}\bar{\mathbf{x}}^*$, with $\bar{\mathbf{x}}$ being the true solution to (4). The mutual coherence μ is defined by $\mu = \max_{i,j} \frac{<\mathbf{B}_i, \mathbf{B}_j>}{||\mathbf{B}_i||||\mathbf{B}_j||}$, with $\mathbf{B}$ being the matrix satisfying $\mathbf{y} = \mathbf{B}\mathbf{X}^\mathbf{S}$, where $\mathbf{X}^\mathbf{S}$ is the vector obtained from stacking the columns of $\mathbf{X}$. The same work also relates other recovery guarantees to the RIP criterion.

In [62] it is shown that for $\mathbf{a}_i$ that are independent, zero-mean normal vectors, on the order of $k^2 \log n$ measurements are sufficient to recover a k-sparse input from measurements of the form (4), using SDP relaxation. In [100], an algorithm is suggested to solve the sparse 1D Fourier phase retrieval problem based on a two-step process, each step cast separately as an SDP problem: First, the support of $\mathbf{x}$ is determined from its autocorrelation sequence, and then $\mathbf{x}$ is determined, given the support. This algorithm is shown experimentally to recover k sparse signals from $O(k^2)$ measurements.

Greedy methods with sparsity prior: Since the matrix lifting algorithms involve a dimension increase, they are not ideally suited for large vectors, where computational cost can become significant. In addition, they are in general not guaranteed to converge to a solution. An alternative to the SDP algorithms is posed by sparsity based greedy algorithms [51], [101], [54]. One algorithm, that is both fast and accurate, is a greedy method named GESPAR (for GrEedy Sparse PhAse Retrieval) [54]. GESPAR attempts to solve the least squares sparse quadratic problem (5). Namely, it seeks a k sparse vector $\mathbf{x}$ consistent with the quadratic measurements $\mathbf{y}$. GESPAR
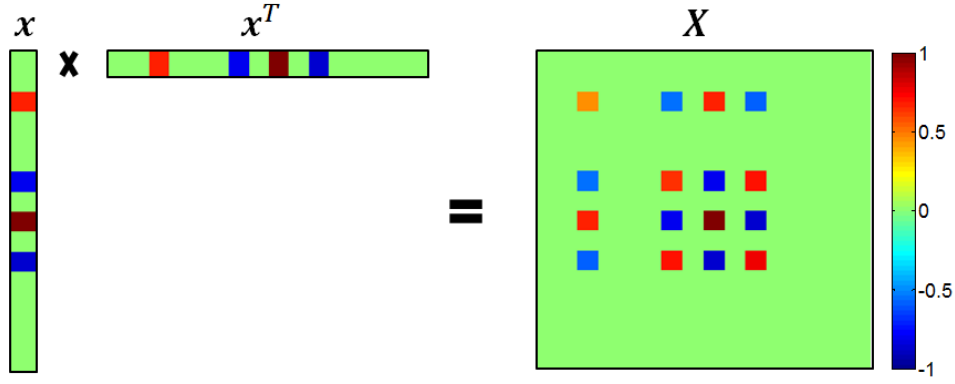
Figure 5.   Sparse vector outer product yields a sparse matrix

is a fast local search method, based on iteratively updating signal support, and seeking a vector that corresponds to the measurements, under the current support constraint. A local-search method is repeatedly invoked, beginning with an initial random support set. Then, at each iteration a swap is performed between a support and an off-support index. Only two elements are changed in the swap (one in the support and one in the off-support), following the so-called *2-opt* method [102]. Given the support of the signal, the phase-retrieval problem is then treated as a non-convex optimization problem, approximated using the damped Gauss Newton method [103]. See Algorithm **2** for a detailed description of the algorithm.

GESPAR has been shown to yield fast and accurate recovery results (see *Sparse phase retrieval algorithms* box and Fig. 6 within), and has been used in several phase-retrieval optics applications - including CDI of 1D objects [104], efficient CDI of sparsely temporally varying objects [55], and phase retrieval via waveguide arrays [56]. A similar method has been used to solve the combined phase-retrieval and sub-wavelength imaging problem [48] (See sub-Section V-D).

Algorithm 2 GESPAR - main steps

Input: $\mathbf{A}_i, y_i, \tau, \text{ITER}$.
$\mathbf{A}_i \in \mathbb{R}^{N \times N}, i = 1, 2, \ldots, M$ - symmetric matrices.
$y_i \in \mathbb{R}, i = 1, 2, \ldots, M$.
τ - threshold parameter.
ITER - Maximum allowed total number of swaps.
Output: $\mathbf{x}$ - an optimal (or suboptimal) solution of (5).

Initialization. Set $T = 0, j = 0$.

1) Generate a random index set $S_0 \ (|S_0| = s)$
2) Invoke the damped Gauss Newton method with support S_0, and obtain an output $\mathbf{z}_0$. Set $\mathbf{x}_0 = \mathbf{U}_{S_0}\mathbf{z}_0$, where $\mathbf{U}_{S_0} \in \mathbb{R}^{N \times s}$ is the matrix consisting of the columns of the identity matrix $\mathbf{I}_N$ corresponding to the index set S_0

General Step $(j = 1, 2, \ldots)$**:**

3) Update support: Let p be the index from S_{j-1} corresponding to the component of $\mathbf{x}_{j-1}$ with the smallest absolute value. Let q be the index from S_{j-1}^c corresponding to the component of $\nabla f(\mathbf{x}_{j-1})$ with the highest absolute value, where $\nabla f(\mathbf{x})$ is the gradient of the least-squares objective function from (5), namely $\nabla f(\mathbf{x}) = 4\sum_i (\mathbf{x}^* \mathbf{A}_i \mathbf{x} - y_i)\mathbf{A}_i\mathbf{x}$. Increase T by 1, and make a swap between the indices p and q, i.e. set $\tilde{S}$ to be:
$$\tilde{S} = (S_{j-1}\backslash\{p\}) \cup \{q\}.$$

4) Minimize with given support: Invoke the damped Gauss Newton method [103] with input $\tilde{S}$ and obtain an output $\tilde{\mathbf{z}}$. Set $\tilde{\mathbf{x}} = \mathbf{U}_S\tilde{\mathbf{z}}$, where $\mathbf{U}_S \in \mathbb{R}^{N \times s}$ is the matrix consisting of the columns of the identity matrix $\mathbf{I}_N$ corresponding to the index set S.
If $f(\tilde{\mathbf{x}}) < f(\mathbf{x}_{j-1})$, then set $S_k = \tilde{S}, \mathbf{x}_k = \tilde{\mathbf{x}}$, advance m and go to 3. If none of the swaps resulted with a better objective function value, go to 1.

Until $f(\mathbf{x}) < \tau$ or $T > \text{ITER}$.
The output is the solution $\mathbf{x}$ that yielded the minimum value for the least-squares objective.

Sparse phase retrieval algorithms - a comparison

We simulate sparse-Fienup [92] and GESPAR [54] for various values of $N \in [64, 2048]$, and $M = 2N$. The recovery probability vs. sparsity k for different vector lengths is shown in Figs. 6a and 6b. In both cases the recovery probability increases with N, while GESPAR clearly outperforms the alternating iteration method.

We then simulate the recovery success rate of three sparsity-based phase retrieval algorithms. We choose $\mathbf{x}$ as a random vector of length $N = 64$. The vector contains uniformly distributed values in the range $[-4, -3] \cup [3, 4]$ in k randomly chosen elements. The $M = 128$ point DFT of the signal is calculated, and its magnitude-square is taken as $\mathbf{y}$, the vector of measurements. In order to recover the unknown vector $\mathbf{x}$, three methods are used: A greedy method (GESPAR[54]), an SDP based method (Algorithm 2, [100]), and an iterative Fienup algorithm with a sparsity constraint ([92]). The Sparse-Fienup algorithm is run using 100 random initial points, out of which the chosen solution is the one that best matches the measurements. Namely, $\hat{\mathbf{x}}$ is selected as the s sparse output of the Sparse-Fienup algorithm with the minimal cost $f(\mathbf{x}) = \sum_{i=1}^{N}(|\mathbf{F}_i\mathbf{x}|^2 - y_i)^2$ out of the 100 runs. The probability of successful recovery is plotted in Fig. 6c for different sparsity levels k. The success probability is defined as the ratio of correctly recovered signals $\mathbf{x}$ out of 100 simulations. In each simulation both the support and the signal values are randomly selected. The three algorithms (GESPAR, SDP and Sparse-Fienup) are compared. The results clearly show that GESPAR outperforms the other methods in terms of probability of successful recovery - over 90% successful recovery up to $k = 15$, vs. $k = 8$ and $k = 7$ in the other two techniques.

For more extensive comparisons, the reader is referred to [54].
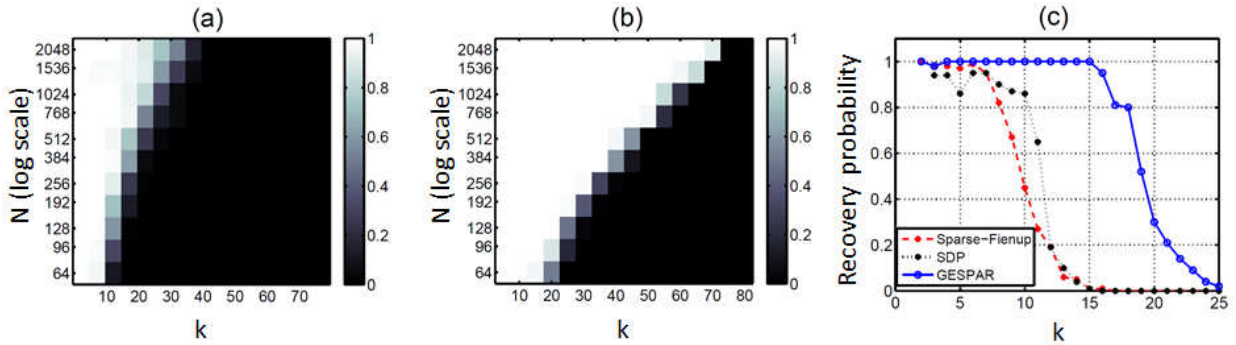

Figure 6. Sparsity-based phase retrieval algorithms, a comparison. (a) Sparse-Fienup recovery probability vs. sparsity k, for various signal length N, and with $M = 2N$. (b) GESPAR recovery probability vs. sparsity k, for various signal length N, and with $M = 2N$. (c) Recovery probability for three algorithms: sparse-Fienup, SDP, and GESPAR for $N = 64$, $M = 128$ [54].

A major advantage of greedy methods over other algorithms (e.g. SDP based) is its low computational cost; GESPAR may be used to find a sparse solution to the 2D Fourier phase retrieval - or phase retrieval of images. Figure 7 shows a recovery example of a sparse 195×195 pixel image, comprised of $s = 15$ circles at random locations and random values on a grid containing 225 points, recovered from its $38,025$ 2D-Fourier magnitude measurements, using GESPAR. The dictionary used in this example contains 225 elements consisting of non-overlapping circles located on a 15×15 point Cartesian grid, each with a 13 pixel diameter. The solution took 80 seconds. Solving the same problem using the sparse Fienup algorithm did not yield a successful reconstruction, and using the SDP method is not practical due to the large matrix sizes.
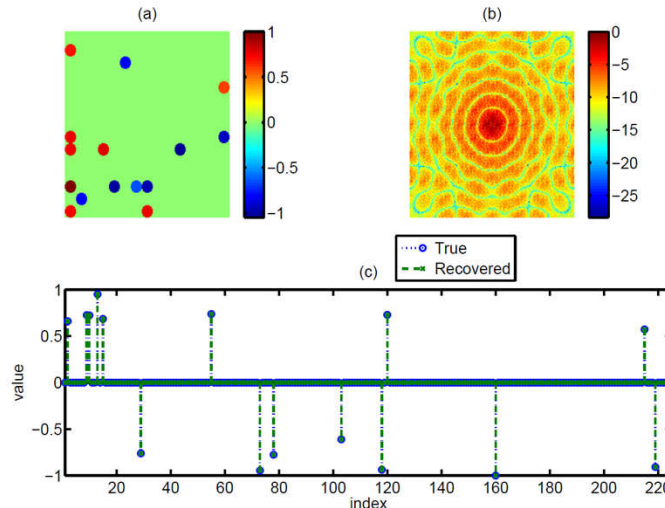

Figure 7. 2D Fourier phase retrieval example. (a) True 195×195 sparse circle image ($s = 15$ circles). (b) Measured 2D Fourier magnitude ($38,025$ measurements, log scale). (c) True and recovered coefficient vectors, corresponding to circle amplitudes at each of the 225 grid points[54].

V. Applications in Lensless Imaging

In this section, we present several CDI applications with connection to the phase retrieval algorithms described in previous sections. The concept of phase retrieval in optical imaging arises from the attempt to recover images from experimental measurements. To this end, it is essential to emphasize that compared to numerical simulations or signal processing of digital data, phase retrieval of experimentally obtained patterns has several additional challenges. First, the far-field intensity distribution (Fourier magnitude) is corrupted by various types of noise, such as Poisson noise, detector read-out noise, and unwanted parasitic scattering from the optics components in the system. Second, in single-shot experiments, the measured far-field intensity distribution is usually incomplete, including a missing center (i.e. the very low spatial frequency information cannot be directly recorded by a detector) [84]. Third, when the far-field intensity distribution is measured by a detector, each pixel integrates the total number of photons within the solid angle subtended by the pixel, which is not exactly equivalent to uniform sampling of the diffraction signal [105]. Additionally, many experiments are carried out using incoherent (but bright) sources. Coherence is achieved by propagating a long distance from the source, but often the experiment is constrained to be carried out with a partially-incoherent beam [106]. All of these issues add complications to algorithmic phase retrieval. However, notwithstanding these challenges, successful phase retrieval of experimental data in optical imaging has been widely achieved [107], [15], [34], [16], [24], [108], [20], [25], [26]. Below, we show several examples.

A. Quantitative comparison of alternating-projection algorithms

Quantitative comparisons between the OSS, HIO, ER-HIO and NR-HIO algorithms have been performed using both simulated and experimental data [14]. Figure 8 shows a noise-free oversampled diffraction pattern (Fourier magnitude squared) calculated from a simulated biological vesicle (Fig. 8c). High Poisson noise was then added to the diffraction intensity (Fig. 8b). Figures 8d-g show the final reconstructions by HIO, ER-HIO, NR-HIO, and OSS, respectively. Visually, OSS produced the most faithful reconstruction among the four algorithms (insets in Fig. 8d-g). The recovery error was quantified using consistency with the measurements:

$$E = \sum_n |z_r[n] - z_m[n]| / \sum_n |z_m[n]| \qquad (21)$$
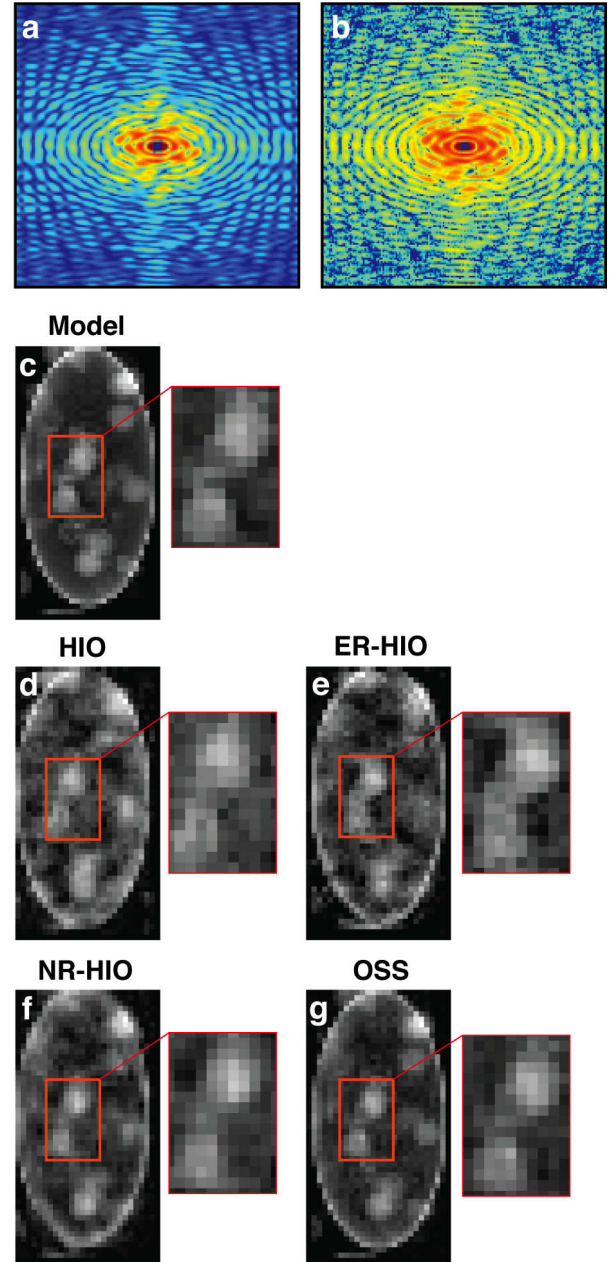

Figure 8. A quantitative comparison between the HIO, ER-HIO, NR-HIO, and OSS algorithms. (a) Noise-free oversampled diffraction pattern calculated from simulated biological vesicle. (b) High Poisson noise added to the oversampled diffraction pattern. (c) The structure model of the biological vesicle and its fine features (inset). The final reconstruction of the noisy diffraction pattern (b) by (d) HIO, (e) ER-HIO, (f) NR-HIO, (g) and OSS [14].

where $z_r[n]$ is the final reconstruction and $z_m[n]$ is the model structure. The value for E of the HIO, ER-HIO, NR-HIO, and OSS reconstructions is $0.28, 0.24, 0.16$ and 0.07, respectively.

Next, the four algorithms were compared using an experimental diffraction pattern measured from a Schizosaccharomyces pombe yeast spore cell [14]. The experiment was conducted on an undulator beamline at a 3rd generation synchrotron radiation (Spring-8) in Japan. A coherent wave of

5 keV X-rays was incident on a fixed, unstained S. pombe yeast spore. An oversampled X-ray diffraction pattern was acquired by a charge-coupled device detector. Figure 9a shows the experimental diffraction pattern in which the centro-square represents the missing low spatial resolution data [86]. By using a loose support, phase retrieval was performed on the measured data with the HIO, ER-HIO, NR-HIO, and OSS algorithms. For each algorithm, five independent trials were conducted, each consisting of 100 independent runs with different random initial phase sets. In each trial, the reconstruction with the smallest error metric R_F was chosen as a final image, where R_F is defined as:

$$R_F = \sum_k \left| |Z_e[k]| - \zeta |Z_r[k]| \right| / \sum_k |Z_e[k]|. \qquad (22)$$

Here $|Z_e[k]|$ is the measured Fourier magnitude, $|Z_m[k]|$ is the recovered Fourier magnitude, and ζ is a scaling factor.

For each algorithm, the mean and average of the five final images were used to quantify the reconstruction. Figures 9c-j show the average and variance of five final images obtained by HIO, ER-HIO [78], NR-HIO [88], and OSS [14], respectively. The average R_F and the consistency of five independent trials are shown in Fig. 9b. Both visual inspection and quantitative results indicate that OSS produced the most consistent reconstructions among all four algorithms.

B. X-ray free electron laser CDI

The majority of imaging experiments at X-ray free-electron laser sources utilize the method of CDI. The lensless nature is actually an advantage when dealing with extremely intense and destructive pulses, where one can only carry out a single pulse measurement with each object (say, a molecule) before the object disintegrates. In such cases, often one cannot use any optical components at all, because any component (e.g., a lens) would be severely damaged by the extremely high flux of (X-ray) photons. CDI solves these problems: it works without the need for optical components. In this vein, CDI also facilitates reliable imaging of moving objects. Indeed, in many experiments the objects move (flow) across the X-ray beam, for example, when the X-ray laser beam hits a focused aerosol beam or nano-particles in a liquid jet. In such an experiment, the particle density is usually adjusted so that the X-ray laser pulse is more likely to hit a single particle than several. A particle is hit by chance by a pulse, but this is not known until the diffraction pattern is read out from the detector, which is done on every pulse. The stream of data is then analyzed

and sorted to give the single-particle hits, which contain the meaningful measured data, while all other data is ignored.

There are two generic classes of these "single particle" CDI experiments: imaging of reproducible particles, and imaging of unique particles. The first category includes particles such as viruses. Assuming that these particles are not aligned in the same direction, the collected data represents diffraction patterns of a common object, but in random orientations. If the orientations can be determined then the full three-dimensional Fourier magnitude of the object can be determined, which in turn could be phased to give a 3D image. A proof of concept of this experiment was carried out by Loh et al [109].

An example of the second class of *flash diffractive imaging* is imaging airborne soot particles in flight in an aerosol beam [26]. Several diffraction patterns of soot particles and clusters of polystyrene spheres (as test objects) are shown in Fig. 10, along with the 2D reconstructions of the objects. The experiments were carried out at the LCLS, using the CFEL-ASG Multi-Purpose (CAMP) instrument [110] at the Atomic, Molecular and Optical Science beam line [111]. Pulses of about 10^{12} photons of 1.0 nm wavelength were focused to an area of 10 μm^2. The X-ray detectors (pnCCD panels) were placed to give a maximum full-period resolution of 13 nm at their center edges.

In these experiments, the phase retrieval of the patterns was carried out using the Relaxed Averaged Alternating Reflections (RAAR) [13] algorithm, and using the Shrinkwrap procedure [112], which determines and iteratively updates the support constraint used. The objects were such that it was possible to apply an additional constraint that the image is real valued. Strikingly, the X-ray coherent diffraction patterns have very high contrast. The intensity minima are close to zero. This has an enormous effect on the ability to recover the phase of these pattern reliably. This reliability is quantified in the phase-retrieval transfer function (PRTF) [18], which compares the magnitude of the complex-valued average of patterns phased with different starting guesses to the square root of the measured diffraction pattern. If, at a particular pixel of the diffraction pattern, the phases are consistently reconstructed, then the sum over N patterns will give a magnitude N times higher than the measured magnitude, and so the PRTF will be unity. If the phases are random, then this sum will tend to zero. For patterns generated with X-Ray free electron lasers, this function is often close to unity and is lower primarily in areas where the signal to noise is low. This limited signal is what ultimately limits the resolution; an estimate of the
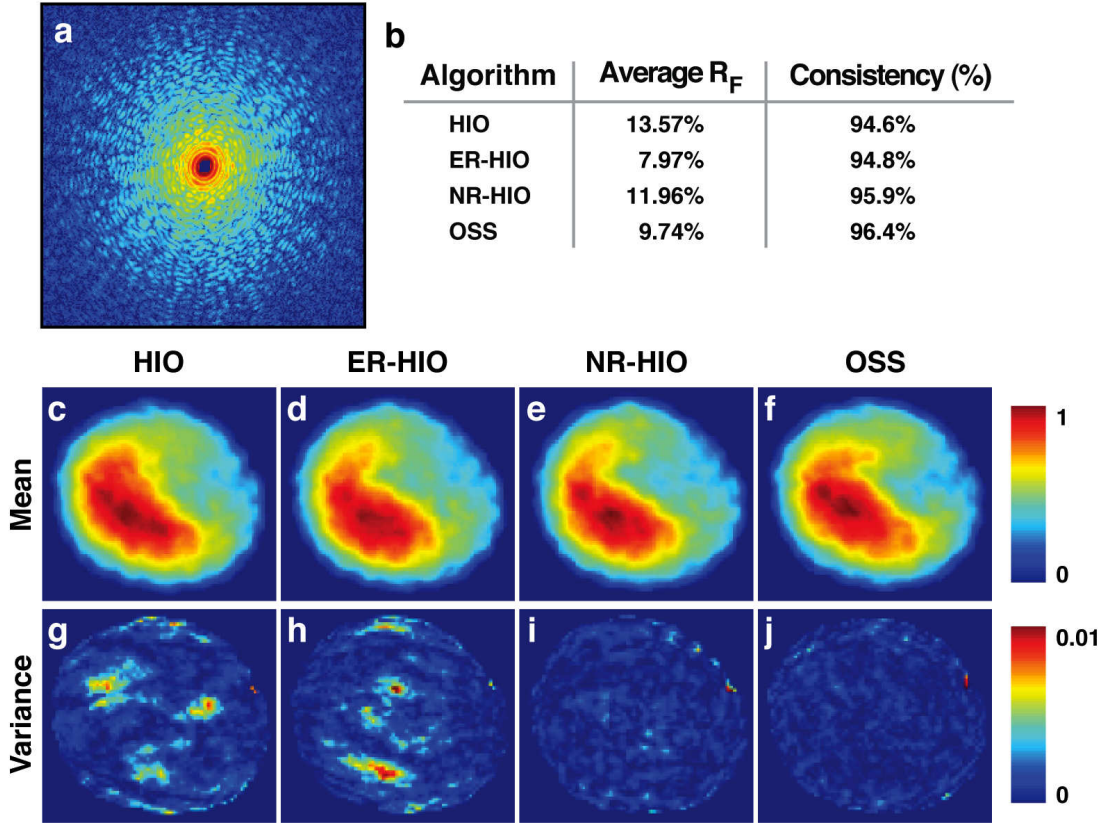
Figure 9. Phase retrieval of an experimental diffraction pattern from a biological sample. (a) Oversampled X-ray diffraction pattern measured from a S. pombe yeast spore cell. (b) The average R_F and the consistency of five independent trials of phase retrieval using four different algorithms. The average reconstruction of five independent trials using HIO (c), ER-HIO (d), NR-HOP (e), and OSS (f). The variance of five final images with HIO (g), ER-HIO (h), NR-HOP (i), and OSS (j). [14]

achieved resolution is given by the white dotted circle on each pattern in Fig. 10. The reconstructed images are sums of ten independent reconstructions. These complex-valued sums have the nice property that the their Fourier spectrum is effectively modulated by the PRTF and hence any artifacts due to noise (or even due to forcibly truncating the data to a lower resolution) is unlikely to show up in the recovered image.

C. Tabletop short wavelength CDI

To-date, most CDI experiments are carried out in 3rd generation synchrotron and X-ray free electron lasers. However, limited access and experimental time hinder the development and applications of CDI using these methods. Thus, over the past several years, CDI microscopes that are based on tabletop sources of coherent extreme UV and soft X-rays are also being developed [113]. Figure 11 shows the first tabletop CDI experiment with extreme UV wavelength.

D. Sub-wavelength CDI using sparsity

Prior knowledge of object-sparsity can help regularize the phase-retrieval problem, as well as compensate for loss of other kinds of information - in this example - the loss of high spatial frequencies. As described before, when an object is illuminated by coherent light of wavelength λ, the far-field intensity pattern is proportional to the magnitude of the object's Fourier transform. In addition, features in the object that are smaller than $\sim \lambda/2$ are smeared due to the diffraction limit. Consequently, the intensity measured in the far field corresponds to $\mathbf{y} \propto |\mathbf{LFx}|^2$ where $\mathbf{L}$ represents a low pass filter at cutoff frequency $\nu_c = 1/\lambda$, $\mathbf{F}$ represents the Fourier transform, and $|\cdot|^2$ stands for elementwise squared absolute value.

Figure 12 (adapted from [48]), shows the recovery of a sparse object containing sub-wavelength features ($100nm$ holes illuminated by a $\lambda = 532nm$ laser) from its experimentally measured low pass filtered Fourier magnitude. The prior knowledge used for recovery is that the object is comprised of a small number of $100nm$ diameter circles on a grid, illuminated by a plane wave. The exact number, locations, and
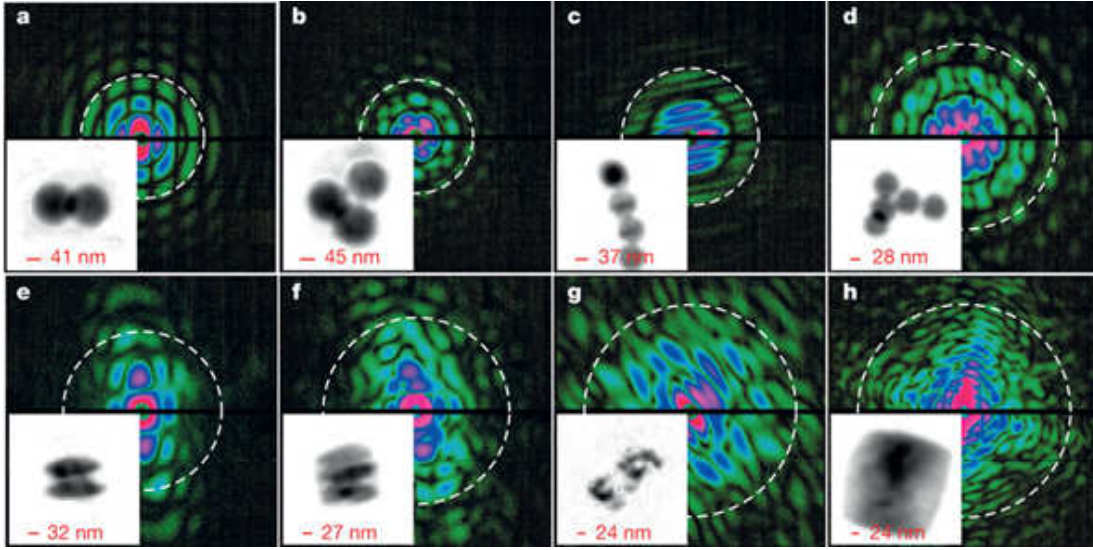
Figure 10. Diffraction patterns from single X-ray FEL pulses from particles in flight, and reconstructed images. a–d, Clusters of polystyrene spheres with radii of 70 nm (a, b) and 44 nm (c, d). e, f, Ellipsoidal nanoparticles. g, A soot particle. h, A salt–soot mixture [26].
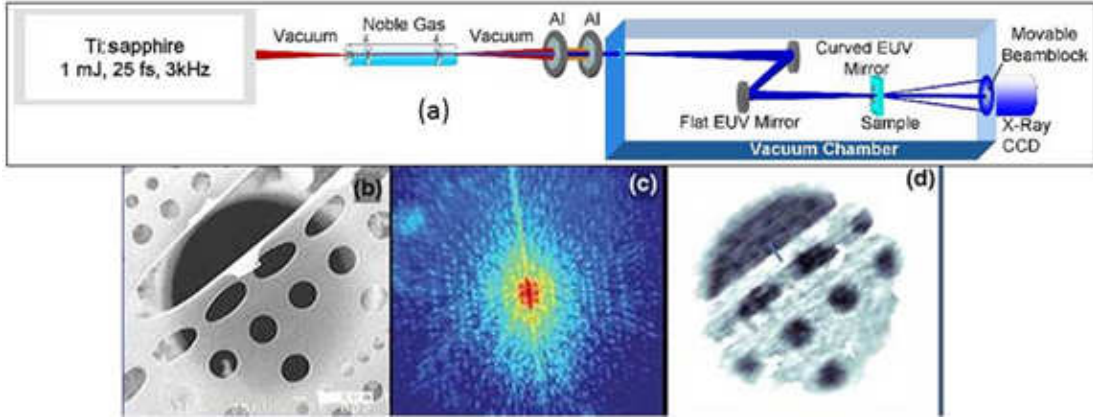

Figure 11. First tabletop short-wavelength coherent diffraction imaging. (a) Experimental setup. Coherent extreme UV radiation is generated through the process of high harmonic generation. A single harmonic order at wavelength 29 nm is selected and focused onto a sample by a pair of multilayer mirrors. The scattered light is detected by X-ray CCD camera. (b) The original image, used to analyze the performance of the CDI process, obtained with a Scanning electron Microscope (SEM). The image shows a masked carbon film placed on a 15 μm diameter pinhole. (c) Recorded multi-frame diffraction pattern (corresponding to Fourier magnitude squared of the object shown in (b)). (d) CDI reconstruction using the HIO algorithm with 214 nm resolution [27].

amplitudes of the circles are not known a-priori. The recovery is performed using a greedy algorithm that iteratively updates the support of the object, finds a local minimum and removes the weakest circle, until convergence [48].

Another type of information loss in CDI, for which the prior knowledge of object sparsity can be helpful, is low signal to noise ratio. In non-destructive X-ray CDI measurements, it is not uncommon for signal acquisition time to be on the order of tens of seconds [27], [114], [30], in order to acheive sufficiently high SNR. This poses a severe limitation on the temporal resolution attainable with such measurements, restricting the types of dynamical phenomena accessible by X-ray CDI. Expoilting sparsity in the *change* that an object undergoes between subsequent CDI frames has been recently suggested as a means to overcome high noise values, and consequently significantly decrease acquisition time [55]. In other words, the fact that an object is *sparsely varying*, can be used as prior information to effectively denoise sequential Fourier magnitude measurements. In [55], CDI of a sparsely varying object is formulated as a sparse quadratic optimization problem, and solved using GESPAR [54]. Numerical simulations suggest a dramatic potential improvement in temporal resolution: In an example consisting of a 51×51 pixel object with 5 randomly varying pixels between frames, an improvement of 2 orders of magnitude in acquisition time is possible [55].
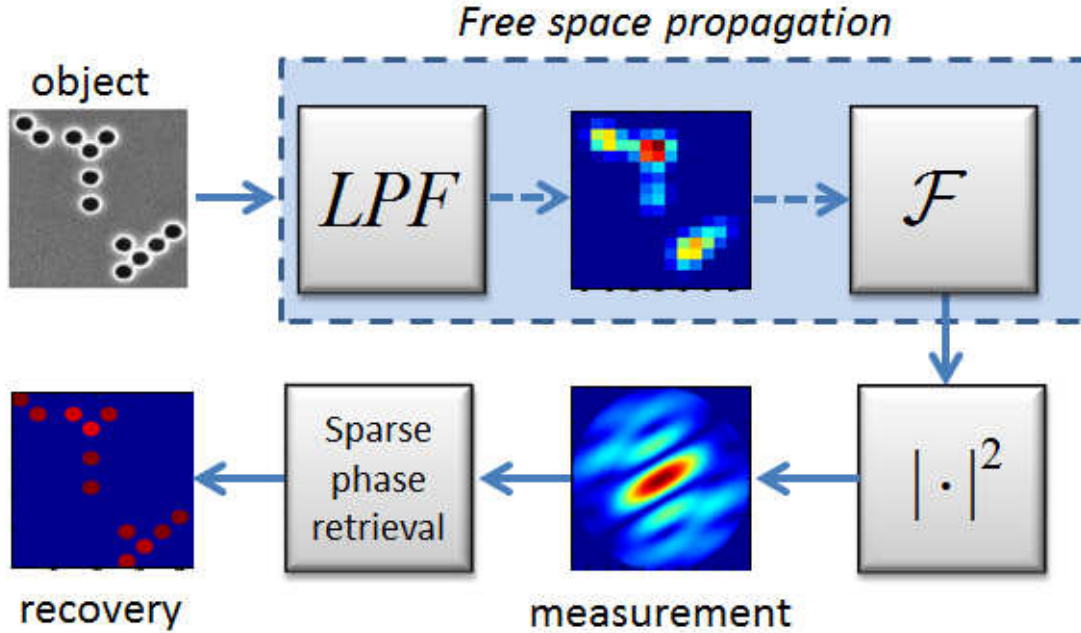
Figure 12. Sparsity based sub-wavelength CDI. A 2D object consisting of an arrangement of nano-holes (100nm in diameter) is illuminated by a 532nm laser, and the Fourier plane magnitude is measured. High spatial frequencies are lost during propagation, because the features (the circles as well as their separation) are smaller than $\sim \lambda/2$. Using an iterative greedy algorithm, and exploiting the prior knowledge that the object is sparse in a dictionary made of 100nm circles, the phase is retrieved and the object is recovered from its low-pass-filtered Fourier magnitude [48].

VI. OTHER PHYSICAL SETTINGS, BOTTLENECKS, AND VISION

This review article focused mainly on the simplest physical setting for phase retrieval in optical imaging (Fig. 2), CDI: where an unknown 2D optical image is recovered algorithmically from a single measurement of its far-field intensity pattern, given a known image support (or other prior information). In terms of signal processing, this problem corresponds to recovering a 2D object from measurements of its Fourier magnitude. However, the issue of phase retrieval in optical imaging, and in a more general sense – in optics, is far broader, and includes other physical settings which naturally translate into signal processing problems different than the standard phase retrieval problem. This section provides a short overview of those physical settings, defines the various problems in terms of signal processing, and provides some key references. We conclude with a discussion on the main challenges and bottlenecks of phase retrieval in optical imaging, followed by an outlook for the upcoming years and long term vision.

A. Non-Fourier Measurements

The simplest optical phase retrieval problem assumes that the measured data corresponds to the Fourier magnitude. In optical settings, this means that the measurements are taken in the Fourier domain of the sought image, which physically means performing the measurements at a plane sufficiently far away from the image plane (the so-called *far-field* or the *Fraunhofer regime*), or at the focal plane of an ideal lens [40]. In reality, however, the measurements can be taken at any plane between the image plane and the far field, which would yield intensity patterns that are very different than the Fourier magnitude of the sought signal. This of course implies that new (or revised) algorithms - beyond those described in previous sections - must be used, which naturally raises issues of conditions for uniqueness and convergence. At the same time, these measurements have some interesting advantages, which can be used wisely to improve the performance of phase retrieval. Let us begin by describing the relevant physical settings.

As stated earlier in this paper, the optical Fourier plane corresponds to a plane sufficiently far away from where the object (the sought signal) is positioned. *Far away* here means asymptotically at infinite distance from the object plane, or at the focal plane of a lens. However, the entire propagation-evolution of electromagnetic waves from any plane to any other plane (not only from the near field to the far field) is known: it is fully described by Maxwell's equations. As such, one can formulate the problem through a proper transfer

function (of the electromagnetic wave) that is different than the Fourier transform. In this context, the most well studied case is the regime of Fresnel diffraction, where the transfer function is expressed in an integral form known as Fresnel integral [40]. This regime occurs naturally at a range of distances away from the object plane which naturally includes also the Fraunhofer regime where the transfer function reduces to a simple Fourier transform. Going beyond the Fresnel regime is also possible. This means that the (magnitude squared of the) electromagnetic wave will be measured at some arbitrary plane away from the object. A more general case arisees by expressing the scalar transfer function of the light in a homogeneous medium, at any plane z as:

$$T(k_x, k_y, z) = \exp\left[-iz\sqrt{k^2 - (k_x^2 + k_y^2)}\right] \qquad (23)$$

Here $k = \omega/c$, with ω being the frequency of the light, c being the speed of light in the medium, and k_x, k_y describe the transverse wavenumbers. The field at any arbitrary plane z, $E(x, y, z)$, is then given by inverse Fourier transforming the spectral function at that plane $F(k_x, k_y, z)$, which is related to the spectrum at the initial plane by:

$$F(k_x, k_y, z) = F(k_x, k_y, z = 0)T(k_x, k_y, z).$$

With the transfer function 23, one can now formulate a new phase retrieval problem, where the measurements are conducted at some arbitrary plane z, giving $|E(x, y, z)|^2$, and the sought signal is $E(x, y, z = 0)$. This approach can be extended to include polarization effects, where the transfer-function is vectorial, thereby describing the propagation through Maxwell's equations with no approximation at all. The optical far-field - where the measurement corresponds to the Fourier magnitude of the image at the initial plane, (i.e., the measurement is proportional to $|F(k_x, k_y, z)|^2$) - is obtained for distances z larger than some minimum distance z_0 that depends on the spectral extent of $F(k_x, k_y, z = 0)$, and only within a region close enough to the z axis in the measurement plane.

It is interesting to compare these more general phase retrieval problems to the generic problem of recovering a signal from its Fourier magnitude. In terms of algorithmics, the generic problem is much simpler and was extensively studied throughout the years, whereas the general case is considerably more complex and was studied only sporadically. However, in terms of optics, the measurements in the general case can provide more information. Namely, in the general case, measurements of $|E(x, y, z)|^2$ can be taken at multiple planes (multiple values of z), and each measurement adds more information on the signal. In contrast, for the generic problem, once the measurements are taken in the optical far-field, taking more measurements at further away distances does not add additional information because all the far field measurements correspond to the Fourier magnitude (to within some known scaling of coordinates in the measurement planes). As such, performing phase retrieval of optical images in the most general (non-Fourier) case can be beneficial, as it leads to multiple measurements, possibly relaxing the conditions on oversampling and/or the advance knowledge on the support in the image plane.

Historically, these ideas on non-Fourier measurements are known to the optics community since the early days of optical phase retrieval [2]. They are currently being used in the context of improving the convergence of phase retrieval by taking non-Fourier measurements at several planes [115], [19]. Alternatively, one can take measurements at several different optical frequencies ω, which would be expressed as different values of $k = \omega/c$ in the general transfer function given above. In this mutli-frequency context, it is important that the frequencies are well separated, each having a narrow bandwidth, to conform the high degree of coherence required for CDI. These ideas are now being pursued by several groups [106], [29], [116]. Interestingly, the multi-frequency idea also works in the continuous case of broad bandwidth pulses centered on a single frequency. In this case, the power spectrum of the pulse must be known in advance [106], [116], [117]. In a similar vein, recent work has demonstrated scanning CDI, where the beam is scanned through overlapping regions on the sample to allow imaging of extended objects, a method known as *ptychography* [118], [119], [20], [120].

More sophisticated physical settings also exist, where the medium within which the waves are propagating is not homogeneous in space. Famous examples are photonic crystals, wherein the refractive index varies periodically in space, in a known fashion, in one, two or three dimensions. Obviously, in such settings the transfer function for electromagnetic waves is fundamentally different from the transfer function in free space. The phase retrieval problem in such systems, albeit less commonly known, is no less important. For example, photonic crystal fibers can in principle be used for imaging in endoscopy. The measurements in such systems correspond to the magnitude squared of the field at the measurement plane, which would be very different than the Fourier magnitude of the sought image. Still, once the transfer function is known,

complicated as it may be, the phase retrieval problem is well defined and can be solved with some modifications to the algorithms described above. See, for example, pioneering work on phase retrieval in a photonic crystal fiber [121], and very recently on sparsity-based phase retrieval and super-resolution in optical waveguide arrays [56]. In addition to these, the concept of CDI has also been extended to other schemes, such as Bragg CDI, suitable to periodic images, to reconstruct the structure and strain of nano-crystals [122], [123], [124], [125].

B. Phase Retrieval Combining Holographic Methods

As explained in the introduction, optical settings always suffer from the inability of photodetectors to directly measure the phase of an electromagnetic wave at frequencies of THz (terahertz) and higher. Partial solution for this problem is provided through holography, invented by Denis Gabor in 1948 [126] and awarded the Nobel Prize in Physics in 1971. Holography involves interfering an electromagnetic field carrying some image, E_{image}, with another electromagnetic field of the same frequency and a known structure, denoted as E_{ref}. Typically, the so-called reference wave, E_{ref}, has a very simply structure, for example, approximately a plane wave (wave of constant amplitude and phase). The detection system records $|E_{image}+E_{ref}|^2$. Originally, such holographic recording was done on a photographic plate which is made from a photosensitive material whose transmission becomes proportional to the recorded pattern $|E_{image} + E_{ref}|^2$. This photographic plate is called a *hologram*, wherein the information contained in the image wave E_{image} is embedded in transmission function of the hologram. To see the recording, the wave of the known pattern, E_{ref}, is generated (which is possible because its structure is simple and fully known) and made to illuminate the hologram. The magnitude of the wave transmitted through the illuminated hologram is therefore proportional to $|E_{image} + E_{ref}|^2 \cdot E_{ref}$. One of the terms is therefore $|E_{ref}|^2 \cdot E_{image}$. Since $|E_{ref}|^2$ carries virtually no information (i.e., it is just a constant), this transmitted wave reconstructs the image times that constant. This is the principle of operation of holography. Over the years, it has been shown that it is almost always beneficial to record not the actual image but its Fourier spectrum, hence the reconstructed information is the Fourier transform of the image, and the image itself is recovered either in the far-field (as explained in the introduction) or at the focal plane of a lens. This process is termed *Fourier holography* [127].

In the context of phase retrieval, holography is used for the purpose of adding information in the measurement scheme. Because in most cases the measurements used are Fourier magnitudes, which physically implies far-field measurements, the natural inclusion of holographic methods is through Fourier holography. For example, adding a tiny hole (a delta function) at a predetermined position in the sample (close to where the sought image resides) creates an additional wave in the far field, with a tilted phase (arising from the displacement between the hole and the sought image). The far field intensity therefore now corresponds to the absolute value squared of the sum of the Fourier spectrum of the sought image and the (known) wave. As such, it introduces additional prior knowledge, which can be used for increased resolution of the algorithmic recovery or for relaxing the constraints on the prior knowledge on the support. These ideas have been exploited successfully using X-rays and electrons by several groups [128], [129], [130].

C. Challenges, Bottlenecks and Vision

The current challenges can be briefly defined in a single sentence: higher resolution, ability to recover more complex objects, improved robustness to noise, and real-time operation. The very reason phase retrieval in optical imaging has become so important is owing to the vision to be able one day to image complex biological molecules directly, track their structural evolution as it evolves in time, and even view the dynamics of the electronic wave functions bonding atoms together. The reasoning is obvious: to understand biology at the molecular level, to decipher the secrets of how their atomic constituents bond together and how they interact with other molecules. The current state of the art is far from those goals: imaging resolution is not yet at the atomic (sub-nanometer) level, and - at nanometric resolution - imaging cannot handle objects that are bounded by a support that is extremely large compared to the resolution. In terms of being able to perform real-time experiments, state of the art measurements have demonstrated extremely short optical pulses: tens of attoseconds (10^{-18} seconds - on the order of the passage of a photon through a distance comparable to the size of an atom). Pioneering experiments have even started to probe the dynamics of electrons in molecules and tunneling processes on these time scales. But, as of today, none of these ultrafast methods was applied to imaging of even a simple molecule, let alone complex biological structures.

Clearly, the underlying physics and engineering pose great challenges to meet these goals. Generating coherent radiation

in the hard X-ray regime is still a major obstacle, often requiring very large enterprises such as the X-ray sources at the SLAC National Accelerator Laboratory. These facilities around the world are continuously improving their photon flux at shorter wavelengths, thereby constantly improving imaging resolution. The fundamental limits on the coherent X-ray flux possible with current methods (such as synchrotrons, XFELs [58], [59], and the process of high harmonics generation [131]) are not even known. But the steady improvement does give hope for imaging at the atomic level in the near future. Taking the CDI techniques to the regime of attosecond science is an important challenge. These pulses are extremely short, hence their bandwidth is huge, so the coherent diffraction pattern is a superposition of their Fourier contents, which requires new algorithmic methods. As described above, these issues are currently being explored by several groups. But the problem is fundamentally more complicated, because the process of scattering of light by molecules at these short wavelengths and ultrashort timescales is not like passing light through a mask on which an image is imprinted. Rather, many issues related to light-matter interactions under these conditions are yet to be understood (e.g., tunneling ionization of atoms by laser pulses).

Finally, the long term vision must include imaging the dynamics within complex biological systems at the atomic level and in real time. But such systems are extremely complex to handle, in terms of details on many spatial and temporal scales simultaneously, in terms of the statistical nature and huge redundancy in the physical processes taking place within such complexes simultaneously, and even in terms of the quantum mechanics governing the dynamics at those scales. This is where the signal processing community can make a large impact, by devising new and original methods for recovering the information from experimental measurements. Clearly, the algorithms will have to be tailored to the specific physical settings.

REFERENCES

[1] D. Sayre, "Some implications of a theorem due to shannon," *Acta Crystallographica*, vol. 5, no. 6, pp. 843–843, Nov. 1952. [Online]. Available: http://scripts.iucr.org/cgi-bin/paper?a00763

[2] J. R. Fienup, "Reconstruction of an object from the modulus of its fourier transform," *Optics Letters*, vol. 3, no. 1, pp. 27–29, Jul. 1978. [Online]. Available: http://ol.osa.org/abstract.cfm?URI=ol-3-1-27

[3] J. Miao, P. Charalambous, J. Kirz, and D. Sayre, "Extending the methodology of x-ray crystallography to allow imaging of micrometre-sized non-crystalline specimens," *Nature*, vol. 400, no. 6742, pp. 342–344, 1999.

[4] M. Howells, T. Beetz, H. Chapman, C. Cui, J. Holton, C. Jacobsen, J. Kirz, E. Lima, S. Marchesini, H. Miao, D. Sayre, D. Shapiro, J. Spence, and D. Starodub, "An assessment of the resolution limitation due to radiation-damage in x-ray diffraction microscopy," *Journal of Electron Spectroscopy and Related Phenomena*, vol. 170, no. 1 - 3, pp. 4 – 12, 2009. [Online]. Available: http://www.sciencedirect.com/science/article/pii/S0368204808001424

[5] D. Sayre and H. Chapman, "X-ray microscopy," *Acta Crystallographica Section A: Foundations of Crystallography*, vol. 51, no. 3, pp. 237–252, 1995.

[6] J. C. Solem and G. C. Baldwin, "Microholography of living organisms," *Science*, vol. 218, no. 4569, pp. 229–235, 1982.

[7] R. Neutze, R. Wouts, D. van der Spoel, E. Weckert, and J. Hajdu, "Potential for biomolecular imaging with femtosecond x-ray pulses," *Nature*, vol. 406, no. 6797, pp. 752–757, 2000.

[8] J. Miao, T. Ishikawa, B. Johnson, E. H. Anderson, B. Lai, and K. O. Hodgson, "High resolution 3d x-ray diffraction microscopy," *Physical review letters*, vol. 89, no. 8, p. 088303, 2002.

[9] J. Spence, U. Weierstall, and M. Howells, "Coherence and sampling requirements for diffractive imaging," *Ultramicroscopy*, vol. 101, no. 2, pp. 149–152, 2004.

[10] V. Elser, "Solution of the crystallographic phase problem by iterated projections," *Acta Crystallographica Section A: Foundations of Crystallography*, vol. 59, no. 3, pp. 201–209, 2003.

[11] S. Marchesini, "Invited article: A unified evaluation of iterative projection algorithms for phase retrieval," *Review of Scientific Instruments*, vol. 78, no. 1, pp. 011301–011301, 2007.

[12] H. H. Bauschke, P. L. Combettes, and D. R. Luke, "Hybrid projection–reflection method for phase retrieval," *JOSA A*, vol. 20, no. 6, pp. 1025–1034, 2003.

[13] D. R. Luke, "Relaxed averaged alternating reflections for diffraction imaging," *Inverse Problems*, vol. 21, no. 1, p. 37, 2005.

[14] J. A. Rodriguez, R. Xu, C.-C. Chen, Y. Zou, and J. Miao, "Oversampling smoothness: an effective algorithm for phase retrieval of noisy diffraction intensities," *Journal of applied crystallography*, vol. 46, no. 2, pp. 312–318, 2013.

[15] I. K. Robinson, I. A. Vartanyants, G. Williams, M. Pfeifer, and J. Pitney, "Reconstruction of the shapes of gold nanocrystals using coherent x-ray diffraction," *Physical Review Letters*, vol. 87, no. 19, p. 195505, 2001.

[16] G. Williams, M. Pfeifer, I. Vartanyants, and I. Robinson, "Three-dimensional imaging of microstructure in au nanocrystals," *Physical review letters*, vol. 90, no. 17, p. 175501, 2003.

[17] J. Miao, K. O. Hodgson, T. Ishikawa, C. A. Larabell, M. A. LeGros, and Y. Nishino, "Imaging whole escherichia coli bacteria by using single-particle x-ray diffraction," *Proceedings of the National Academy of Sciences*, vol. 100, no. 1, pp. 110–112, 2003.

[18] H. N. Chapman, A. Barty, S. Marchesini, A. Noy, S. P. Hau-Riege, C. Cui, M. R. Howells, R. Rosen, H. He, J. C. Spence *et al.*, "High-resolution ab initio three-dimensional x-ray diffraction microscopy," *JOSA A*, vol. 23, no. 5, pp. 1179–1200, 2006.

[19] B. Abbey, K. A. Nugent, G. J. Williams, J. N. Clark, A. G. Peele, M. A. Pfeifer, M. De Jonge, and I. McNulty, "Keyhole coherent diffractive imaging," *Nature Physics*, vol. 4, no. 5, pp. 394–398, 2008.

[20] M. Dierolf, A. Menzel, P. Thibault, P. Schneider, C. M. Kewish, R. Wepf, O. Bunk, and F. Pfeiffer, "Ptychographic x-ray computed tomography at the nanoscale," *Nature*, vol. 467, no. 7314, pp. 436–439, 2010.

[21] D. Nam, J. Park, M. Gallagher-Jones, S. Kim, Y. Kohmura, H. Naitow, N. Kunishima, T. Yoshida, T. Ishikawa, C. Song *et al.*, "Imaging

fully hydrated whole cells by coherent x-ray diffraction microscopy." *Physical review letters*, vol. 110, no. 9, pp. 098 103–098 103, 2013.

[22] A. Barty, S. Boutet, M. J. Bogan, S. Hau-Riege, S. Marchesini, K. Sokolowski-Tinten, N. Stojanovic, R. Tobey, H. Ehrke, A. Cavalleri, S. DÃŒsterer, M. Frank, S. Bajt, B. W. Woods, M. M. Seibert, J. Hajdu, R. Treusch, and H. N. Chapman, "Ultrafast single-shot diffraction imaging of nanoscale dynamics," *Nature Photonics*, vol. 2, no. 7, pp. 415–419, 2008. [Online]. Available: http://www.nature.com/nphoton/journal/v2/n7/abs/nphoton.2008.128.html

[23] A. Mancuso, A. Schropp, B. Reime, L.-M. Stadler, A. Singer, J. Gulden, S. Streit-Nierobisch, C. Gutt, G. Grübel, J. Feldhaus *et al.*, "Coherent-pulse 2d crystallography using a free-electron laser x-ray source," *Physical review letters*, vol. 102, no. 3, p. 035502, 2009.

[24] H. N. Chapman, A. Barty, M. J. Bogan, S. Boutet, M. Frank, S. P. Hau-Riege, S. Marchesini, B. W. Woods, S. Bajt, W. H. Benner *et al.*, "Femtosecond diffractive imaging with a soft-x-ray free-electron laser," *Nature Physics*, vol. 2, no. 12, pp. 839–843, 2006.

[25] M. M. Seibert, T. Ekeberg, F. R. N. C. Maia, M. Svenda, J. Andreasson, O. Jonsson, D. Odic, B. Iwan, A. Rocker, D. Westphal, M. Hantke, D. P. DePonte, A. Barty, J. Schulz, L. Gumprecht, N. Coppola, A. Aquila, M. Liang, T. A. White, A. Martin, C. Caleman, S. Stern, C. Abergel, V. Seltzer, J.-M. Claverie, C. Bostedt, J. D. Bozek, S. Boutet, A. A. Miahnahri, M. Messerschmidt, J. Krzywinski, G. Williams, K. O. Hodgson, M. J. Bogan, C. Y. Hampton, R. G. Sierra, D. Starodub, I. Andersson, S. Bajt, M. Barthelmess, J. C. H. Spence, P. Fromme, U. Weierstall, R. Kirian, M. Hunter, R. B. Doak, S. Marchesini, S. P. Hau-Riege, M. Frank, R. L. Shoeman, L. Lomb, S. W. Epp, R. Hartmann, D. Rolles, A. Rudenko, C. Schmidt, L. Foucar, N. Kimmel, P. Holl, B. Rudek, B. Erk, A. Homke, C. Reich, D. Pietschner, G. Weidenspointner, L. Struder, G. Hauser, H. Gorke, J. Ullrich, I. Schlichting, S. Herrmann, G. Schaller, F. Schopper, H. Soltau, K.-U. Kuhnel, R. Andritschke, C.-D. Schroter, F. Krasniqi, M. Bott, S. Schorb, D. Rupp, M. Adolph, T. Gorkhover, H. Hirsemann, G. Potdevin, H. Graafsma, B. Nilsson, H. N. Chapman, and J. Hajdu, "Single mimivirus particles intercepted and imaged with an x-ray laser," *Nature*, vol. 470, no. 7332, pp. 78–81, Feb. 2011. [Online]. Available: http://dx.doi.org/10.1038/nature09748

[26] N. D. Loh, C. Y. Hampton, A. V. Martin, D. Starodub, R. G. Sierra, A. Barty, A. Aquila, J. Schulz, L. Lomb, J. Steinbrener, R. L. Shoeman, S. Kassemeyer, C. Bostedt, J. Bozek, S. W. Epp, B. Erk, R. Hartmann, D. Rolles, A. Rudenko, B. Rudek, L. Foucar, N. Kimmel, G. Weidenspointner, G. Hauser, P. Holl, E. Pedersoli, M. Liang, M. S. Hunter, L. Gumprecht, N. Coppola, C. Wunderer, H. Graafsma, F. R. N. C. Maia, T. Ekeberg, M. Hantke, H. Fleckenstein, H. Hirsemann, K. Nass, T. A. White, H. J. Tobias, G. R. Farquar, W. H. Benner, S. P. Hau-Riege, C. Reich, A. Hartmann, H. Soltau, S. Marchesini, S. Bajt, M. Barthelmess, P. Bucksbaum, K. O. Hodgson, L. StrÃŒder, J. Ullrich, M. Frank, I. Schlichting, H. N. Chapman, and M. J. Bogan, "Fractal morphology, imaging and mass spectrometry of single aerosol particles in flight," *Nature*, vol. 486, no. 7404, pp. 513–517, Jun. 2012. [Online]. Available: http://www.nature.com/nature/journal/v486/n7404/abs/nature11222.html

[27] R. L. Sandberg, A. Paul, D. A. Raymondson, S. HÃ€drich, D. M. Gaudiosi, J. Holtsnider, R. I. Tobey, O. Cohen, M. M. Murnane, H. C. Kapteyn, C. Song, J. Miao, Y. Liu, and F. Salmassi, "Lensless diffractive imaging using tabletop coherent high-harmonic soft-x-ray beams," *Physical Review Letters*, vol. 99, no. 9, p. 098103, Aug. 2007. [Online]. Available: http://link.aps.org/doi/10.1103/PhysRevLett.99.098103

[28] A. Ravasio, D. Gauthier, F. Maia, M. Billon, J. Caumes, D. Garzella, M. Géléoc, O. Gobert, J.-F. Hergott, A. Pena *et al.*, "Single-shot diffractive imaging with a table-top femtosecond soft x-ray laser-harmonics source," *Physical review letters*, vol. 103, no. 2, p. 028104, 2009.

[29] B. Chen, R. A. Dilanian, S. Teichmann, B. Abbey, A. G. Peele, G. J. Williams, P. Hannaford, L. Van Dao, H. M. Quiney, and K. A. Nugent, "Multiple wavelength diffractive imaging," *PHYSICAL REVIEW A: atomic, molecular, and optical physics*, vol. 79, no. 2, p. 23809, 2009.

[30] M. D. Seaberg, D. E. Adams, E. L. Townsend, D. A. Raymondson, W. F. Schlotter, Y. Liu, C. S. Menoni, L. Rong, C.-C. Chen, J. Miao, H. C. Kapteyn, and M. M. Murnane, "Ultrahigh 22 nm resolution coherent diffractive imaging using a desktop 13 nm high harmonic source," *Optics Express*, vol. 19, no. 23, pp. 22 470–22 479, Nov. 2011. [Online]. Available: http://www.opticsexpress.org/abstract.cfm?URI=oe-19-23-22470

[31] R. L. Sandberg, C. Song, P. W. Wachulak, D. A. Raymondson, A. Paul, B. Amirbekian, E. Lee, A. E. Sakdinawat, L.-O. Chan, M. C. Marconi *et al.*, "High numerical aperture tabletop soft x-ray diffraction microscopy with 70-nm resolution," *Proceedings of the National Academy of Sciences*, vol. 105, no. 1, pp. 24–27, 2008.

[32] J. Bertolotti, E. G. van Putten, C. Blum, A. Lagendijk, W. L. Vos, and A. P. Mosk, "Non-invasive imaging through opaque scattering layers," *Nature*, vol. 491, no. 7423, pp. 232–234, 2012.

[33] J. Miao, T. Ohsuna, O. Terasaki, K. O. Hodgson, and M. A. O'Keefe, "Atomic resolution three-dimensional electron diffraction microscopy," *Physical review letters*, vol. 89, no. 15, p. 155502, 2002.

[34] J. Zuo, I. Vartanyants, M. Gao, R. Zhang, and L. Nagahara, "Atomic resolution imaging of a carbon nanotube from diffraction intensities," *Science*, vol. 300, no. 5624, pp. 1419–1421, 2003.

[35] C. T. Putkunz, A. J. D'Alfonso, A. J. Morgan, M. Weyland, C. Dwyer, L. Bourgeois, J. Etheridge, A. Roberts, R. E. Scholten, K. A. Nugent *et al.*, "Atom-scale ptychographic electron diffractive imaging of boron nitride cones," *Physical Review Letters*, vol. 108, no. 7, p. 073901, 2012.

[36] P. Thibault and V. Elser, "X-ray diffraction microscopy," *Annu. Rev. Condens. Matter Phys.*, vol. 1, no. 1, pp. 237–255, 2010.

[37] K. A. Nugent, "Coherent methods in the x-ray sciences," *Advances in Physics*, vol. 59, no. 1, pp. 1–99, 2010.

[38] J. Miao, K. O. Hodgson, and D. Sayre, "An approach to three-dimensional structures of biomolecules by using single-molecule diffraction images," *Proceedings of the National Academy of Sciences*, vol. 98, no. 12, pp. 6641–6645, 2001.

[39] C. Song, H. Jiang, A. Mancuso, B. Amirbekian, L. Peng, R. Sun, S. S. Shah, Z. H. Zhou, T. Ishikawa, and J. Miao, "Quantitative imaging of single, unstained viruses with coherent x rays," *Physical review letters*, vol. 101, no. 15, p. 158101, 2008.

[40] B. E. A. Saleh and M. C. Teich, *Fundamentals of Photonics*. John Wiley & Sons, Mar. 2007.

[41] E. J. Candes, T. Strohmer, and V. Voroninski, "PhaseLift: exact and stable signal recovery from magnitude measurements via convex programming," *Communications on Pure and Applied Mathematics*, 2012.

[42] E. J. Candes, Y. C. Eldar, T. Strohmer, and V. Voroninski, "Phase retrieval via matrix completion," *SIAM Journal on Imaging Sciences*, vol. 6, no. 1, pp. 199–225, 2013.

[43] R. Balan, P. Casazza, and D. Edidin, "On signal reconstruction without phase," *Applied and Computational Harmonic Analysis*, vol. 20, no. 3, pp. 345–356, 2006.

[44] M. L. Moravec, J. K. Romberg, and R. G. Baraniuk, "Compressive phase retrieval," in *Optical Engineering+ Applications*. International Society for Optics and Photonics, 2007, pp. 670 120–670 120.

[45] A. Fannjiang, "Absolute uniqueness of phase retrieval with random illumination," *Inverse Problems*, vol. 28, no. 7, p. 075008, 2012.

[46] A. S. Bandeira, J. Cahill, D. G. Mixon, and A. A. Nelson, "Saving phase: Injectivity and stability for phase retrieval," arXiv e-print 1302.4618, Feb. 2013. [Online]. Available: http://arxiv.org/abs/1302.4618

[47] A. Beck and Y. C. Eldar, "Sparsity constrained nonlinear optimization: Optimality conditions and algorithms," *SIAM Journal on Optimization*, vol. 23, no. 3, pp. 1480–1509, 2013. [Online]. Available: http://epubs.siam.org/doi/abs/10.1137/120869778

[48] A. Szameit, Y. Shechtman, E. Osherovich, E. Bullkich, P. Sidorenko, H. Dana, S. Steiner, E. B. Kley, S. Gazit, T. Cohen-Hyams, S. Shoham, M. Zibulevsky, I. Yavneh, Y. C. Eldar, O. Cohen, and M. Segev, "Sparsity-based single-shot subwavelength coherent diffractive imaging," *Nature Materials*, vol. 11, no. 5, pp. 455–459, 2012. [Online]. Available: http://www.nature.com/nmat/journal/v11/n5/full/nmat3289.html

[49] Y. Shechtman, Y. C. Eldar, A. Szameit, and M. Segev, "Sparsity based sub-wavelength imaging with partially incoherent light via quadratic compressed sensing," *Optics Express*, vol. 19, no. 16, pp. 14 807–14 822, Aug. 2011. [Online]. Available: http://www.opticsexpress.org/abstract.cfm?URI=oe-19-16-14807

[50] H. Ohlsson, A. Yang, R. Dong, and S. Sastry, "Compressive phase retrieval from squared output measurements via semidefinite programming," *arXiv preprint arXiv:1111.6323*, 2011.

[51] S. Bahmani, P. Boufounos, and B. Raj, "Greedy sparsity-constrained optimization," in *Signals, Systems and Computers (ASILOMAR), 2011 Conference Record of the Forty Fifth Asilomar Conference on*, 2011, pp. 1148–1152.

[52] K. Jaganathan, S. Oymak, and B. Hassibi, "Recovery of sparse 1-d signals from the magnitudes of their fourier transform," in *2012 IEEE International Symposium on Information Theory Proceedings (ISIT)*, 2012, pp. 1473–1477.

[53] Y. C. Eldar and S. Mendelson, "Phase retrieval: Stability and recovery guarantees," *Applied and Computational Harmonic Analysis*, no. 0, pp. –, 2013. [Online]. Available: http://www.sciencedirect.com/science/article/pii/S1063520313000717

[54] Y. Shechtman, A. Beck, and Y. C. Eldar, "GESPAR: efficient phase retrieval of sparse signals," *arXiv preprint arXiv:1301.1018*, 2013.

[55] Y. Shechtman, Y. C. Eldar, O. Cohen, and M. Segev, "Efficient coherent diffractive imaging for sparsely varying objects," *Optics Express*, vol. 21, no. 5, pp. 6327–6338, Mar. 2013. [Online]. Available: http://www.opticsexpress.org/abstract.cfm?URI=oe-21-5-6327

[56] Y. Shechtman, E. Small, Y. Lahini, M. Verbin, Y. C. Eldar, Y. Silberberg, and M. Segev, "Sparsity-based super-resolution and phase-retrieval in waveguide arrays," *Opt. Express*, vol. 21, no. 20, pp. 24 015–24 024, Oct 2013. [Online]. Available: http://www.opticsexpress.org/abstract.cfm?URI=oe-21-20-24015

[57] Y. C. Eldar and G. Kutyniok, *Compressed Sensing: Theory and Applications*. Cambridge University Press, 2012.

[58] P. Emma, R. Akre, J. Arthur, R. Bionta, C. Bostedt, J. Bozek, A. Brachmann, P. Bucksbaum, R. Coffee, F.-J. Decker *et al.*, "First lasing and operation of an ångstrom-wavelength free-electron laser," *nature photonics*, vol. 4, no. 9, pp. 641–647, 2010.

[59] T. Ishikawa, H. Aoyagi, T. Asaka, Y. Asano, N. Azumi, T. Bizen, H. Ego, K. Fukami, T. Fukui, Y. Furukawa *et al.*, "A compact x-ray free-electron laser emitting in the sub-angstrom region," *Nature Photonics*, vol. 6, no. 8, pp. 540–544, 2012.

[60] I. Waldspurger, A. d'Aspremont, and S. Mallat, "Phase recovery, maxcut and complex semidefinite programming," *arXiv preprint arXiv:1206.0102*, 2012.

[61] P. Netrapalli, P. Jain, and S. Sanghavi, "Phase retrieval using alternating minimization," *arXiv preprint arXiv:1306.0160*, 2013.

[62] X. Li and V. Voroninski, "Sparse signal recovery from quadratic measurements via convex programming," *arXiv preprint arXiv:1209.4785*, 2012.

[63] D. Gross, F. Krahmer, and R. Kueng, "A partial derandomization of phaselift using spherical designs," *arXiv preprint arXiv:1310.2267*, 2013.

[64] A. V. Oppenheim and J. S. Lim, "The importance of phase in signals," *Proceedings of the IEEE*, vol. 69, no. 5, pp. 529–541, 1981.

[65] E. Hofstetter, "Construction of time-limited functions with specified autocorrelation functions," *Information Theory, IEEE Transactions on*, vol. 10, no. 2, pp. 119–126, 1964.

[66] Y. M. Bruck and L. Sodin, "On the ambiguity of the image reconstruction problem," *Optics Communications*, vol. 30, no. 3, pp. 304–308, 1979.

[67] M. Hayes, "The reconstruction of a multidimensional sequence from the phase or magnitude of its fourier transform," *IEEE Transactions on Acoustics, Speech and Signal Processing*, vol. 30, no. 2, pp. 140–154, 1982.

[68] R. Bates *et al.*, "Fourier phase problems are uniquely solvable in more than one dimension. i: Underlying theory," *Optik*, vol. 61, no. 3, pp. 247–262, 1982.

[69] J. Miao, D. Sayre, and H. Chapman, "Phase retrieval from the magnitude of the fourier transforms of nonperiodic objects," *JOSA A*, vol. 15, no. 6, pp. 1662–1669, 1998.

[70] P. Van Hove, M. Hayes, J. Lim, and A. Oppenheim, "Signal reconstruction from signed fourier transform magnitude," *Acoustics, Speech and Signal Processing, IEEE Transactions on*, vol. 31, no. 5, pp. 1286–1293, 1983.

[71] M. Elad, *Sparse and redundant representations: from theory to applications in signal and image processing*. Springer Verlag, 2010.

[72] J. Ranieri, A. Chebira, Y. M. Lu, and M. Vetterli, "Phase retrieval for sparse signals: Uniqueness conditions," *arXiv preprint arXiv:1308.3058*, 2013.

[73] H. Ohlsson and Y. C. Eldar, "On conditions for uniqueness in sparse phase retrieval," *arXiv preprint arXiv:1308.5447*, 2013.

[74] K. Jaganathan, S. Oymak, and B. Hassibi, "Sparse phase retrieval: Uniqueness guarantees and recovery algorithms," *arXiv:1311.2745 [cs, math]*, Nov. 2013. [Online]. Available: http://arxiv.org/abs/1311.2745

[75] E. Osherovich, M. Zibulevsky, and I. Yavneh, "Approximate fourier phase information in the phase retrieval problem: what it gives and how to use it," *JOSA A*, vol. 28, no. 10, pp. 2124–2131, 2011.

[76] E. Candes, X. Li, and M. Soltanolkotabi, "Phase retrieval from masked fourier transforms," *arXiv preprint arXiv:1310.3240*, 2013.

[77] R. Gerchberg and W. Saxton, "A practical algorithm for the determination of phase from image and diffraction plane pictures," *Optik*, vol. 35, p. 237, 1972.

[78] J. Fienup, "Phase retrieval algorithms: a comparison," *Applied optics*, vol. 21, no. 15, pp. 2758–2769, 1982.

[79] N. Streibl, "Phase imaging by the transport equation of intensity," *Optics Communications*, vol. 49, no. 1, pp. 6 – 10, 1984. [Online]. Available: http://www.sciencedirect.com/science/article/pii/0030401884900798

[80] M. Soto and E. Acosta, "Improved phase imaging from intensity measurements in multiple planes," *Applied optics*, vol. 46, no. 33, pp. 7978–7981, 2007.

[81] W. Hoppe and G. Strube, "Beugung in inhomogenen primarstrahlenwellenfeld. II. lichtoptische analogieversuche zur phasenmessung von gitterinterferenzen," *Acta Crystallographica Section A: Crystal Physics,*

Diffraction, Theoretical and General Crystallography, vol. 25, no. 4, pp. 502–507, 1969.

[82] J. Rodenburg, "Ptychography and related diffractive imaging methods," *Advances in Imaging and Electron Physics*, vol. 150, pp. 87–184, 2008.

[83] J. R. Fienup, "Reconstruction of a complex-valued object from the modulus of its fourier transform using a support constraint," *J. Opt. Soc. Am. A*, vol. 4, no. 1, pp. 118–123, Jan 1987. [Online]. Available: http://josaa.osa.org/abstract.cfm?URI=josaa-4-1-118

[84] J. Miao, Y. Nishino, Y. Kohmura, B. Johnson, C. Song, S. H. Risbud, and T. Ishikawa, "Quantitative image reconstruction of gan quantum dots from oversampled diffraction intensities alone," *Physical review letters*, vol. 95, no. 8, p. 085503, 2005.

[85] J. Miao, C.-C. Chen, C. Song, Y. Nishino, Y. Kohmura, T. Ishikawa, D. Ramunno-Johnson, T.-K. Lee, and S. H. Risbud, "Three-dimensional gan-ga_ {2} o_ {3} core shell structure revealed by x-ray diffraction microscopy," *Physical review letters*, vol. 97, no. 21, p. 215503, 2006.

[86] H. Jiang, C. Song, C.-C. Chen, R. Xu, K. S. Raines, B. P. Fahimian, C.-H. Lu, T.-K. Lee, A. Nakashima, J. Urano *et al.*, "Quantitative 3d imaging of whole, unstained cells by using x-ray diffraction microscopy," *Proceedings of the National Academy of Sciences*, vol. 107, no. 25, pp. 11 234–11 239, 2010.

[87] C. Chen, J. Miao, C. Wang, and T. Lee, "Application of optimization technique to noncrystalline x-ray diffraction microscopy: Guided hybrid input-output method," *PHYSICAL REVIEW-SERIES B-*, vol. 76, no. 6, p. 064113, 2007.

[88] A. V. Martin, F. Wang, N. D. Loh, T. Ekeberg, F. R. N. C. Maia, M. Hantke, G. van der Schot, C. Y. Hampton, R. G. Sierra, A. Aquila, S. Bajt, M. Barthelmess, C. Bostedt, J. D. Bozek, N. Coppola, S. W. Epp, B. Erk, H. Fleckenstein, L. Foucar, M. Frank, H. Graafsma, L. Gumprecht, A. Hartmann, R. Hartmann, G. Hauser, H. Hirsemann, P. Holl, S. Kassemeyer, N. Kimmel, M. Liang, L. Lomb, S. Marchesini, K. Nass, E. Pedersoli, C. Reich, D. Rolles, B. Rudek, A. Rudenko, J. Schulz, R. L. Shoeman, H. Soltau, D. Starodub, J. Steinbrener, F. Stellato, L. Strüder, J. Ullrich, G. Weidenspointner, T. A. White, C. B. Wunderer, A. Barty, I. Schlichting, M. J. Bogan, and H. N. Chapman, "Noise-robust coherent diffractive imaging with a single diffraction pattern," *Opt. Express*, vol. 20, no. 15, pp. 16 650–16 661, Jul 2012. [Online]. Available: http://www.opticsexpress.org/abstract.cfm?URI=oe-20-15-16650

[89] H. Bauschke, P. Combettes, and D. Luke, "Phase retrieval, error reduction algorithm, and fienup variants: a view from convex optimization," *JOSA A*, vol. 19, no. 7, pp. 1334–1345, 2002.

[90] L. Vandenberghe and S. Boyd, "Semidefinite programming," *SIAM review*, vol. 38, no. 1, pp. 49–95, 1996.

[91] M. Fazel, H. Hindi, and S. P. Boyd, "Log-det heuristic for matrix rank minimization with applications to hankel and euclidean distance matrices," in *American Control Conference, 2003. Proceedings of the 2003*, vol. 3. IEEE, 2003, pp. 2156–2162.

[92] S. Mukherjee and C. Seelamantula, "An iterative algorithm for phase retrieval with sparsity constraints: application to frequency domain optical coherence tomography," in *Acoustics, Speech and Signal Processing (ICASSP), 2012 IEEE International Conference on*, 2012, pp. 553–556.

[93] E. Candes, J. Romberg, and T. Tao, "Robust uncertainty principles: exact signal reconstruction from highly incomplete frequency information," *IEEE Transactions on Information Theory*, vol. 52, no. 2, pp. 489 – 509, Feb. 2006.

[94] D. Donoho, "Compressed sensing," *IEEE Transactions on Information Theory*, vol. 52, no. 4, pp. 1289–1306, 2006.

[95] D. L. Donoho and M. Elad, "Optimally sparse representation in general (nonorthogonal) dictionaries via l1 minimization," *Proceedings of the National Academy of Sciences*, vol. 100, no. 5, pp. 2197–2202, Mar. 2003, PMID: 16576749. [Online]. Available: http://www.pnas.org/content/100/5/2197

[96] Y. C. Pati, R. Rezaiifar, and P. Krishnaprasad, "Orthogonal matching pursuit: Recursive function approximation with applications to wavelet decomposition," in *Signals, Systems and Computers, 1993. 1993 Conference Record of The Twenty-Seventh Asilomar Conference on*. IEEE, 1993, pp. 40–44.

[97] S. S. Chen, D. L. Donoho, and M. A. Saunders, "Atomic decomposition by basis pursuit," *SIAM Journal on Scientific Computing*, vol. 20, no. 1, pp. 33–61, Jan. 1998. [Online]. Available: http://epubs.siam.org/doi/abs/10.1137/S1064827596304010

[98] E. Candes and T. Tao, "Decoding by linear programming," *IEEE Transactions on Information Theory*, vol. 51, no. 12, pp. 4203–4215, 2005.

[99] M. F. Duarte and Y. C. Eldar, "Structured compressed sensing: From theory to applications," *Signal Processing, IEEE Transactions on*, vol. 59, no. 9, pp. 4053–4085, 2011.

[100] K. Jaganathan, S. Oymak, and B. Hassibi, "Recovery of sparse 1-d signals from the magnitudes of their fourier transform," *CoRR*, vol. abs/1206.1405, 2012.

[101] A. Beck and Y. C. Eldar, "Sparsity constrained nonlinear optimization: Optimality conditions and algorithms," *arXiv:1203.4580*, Mar. 2012. [Online]. Available: http://arxiv.org/abs/1203.4580

[102] C. H. Papadimitriou and K. Steiglitz, *Combinatorial optimization: algorithms and complexity*. Courier Dover Publications, 1998.

[103] D. P. Bertsekas, "Nonlinear programming," 1999.

[104] P. Sidorenko, A. Fleischer, Y. Shechtman, Y. C. Eldar, M. Segev, and O. Cohen, "Sparsity-based super-resolution coherent diffractive imaging of (practically) 1d images using extreme uv radiation," in *CLEO: 2013*. Optical Society of America, 2013, p. QF1C.7.

[105] C. Song, D. Ramunno-Johnson, Y. Nishino, Y. Kohmura, T. Ishikawa, C.-C. Chen, T.-K. Lee, and J. Miao, "Phase retrieval from exactly oversampled diffraction intensity through deconvolution," *Physical Review B*, vol. 75, no. 1, p. 012102, 2007.

[106] L. Whitehead, G. Williams, H. Quiney, D. Vine, R. Dilanian, S. Flewett, K. Nugent, A. Peele, E. Balaur, and I. McNulty, "Diffractive imaging using partially coherent x rays," *Physical review letters*, vol. 103, no. 24, p. 243902, 2009.

[107] J. Miao, P. Charalambous, J. Kirz, and D. Sayre, "Extending the methodology of x-ray crystallography to allow imaging of micrometre-sized non-crystalline specimens," *Nature*, vol. 400, no. 6742, pp. 342–344, Jul. 1999. [Online]. Available: http://www.nature.com/nature/journal/v400/n6742/abs/400342a0.html

[108] C. Song, H. Jiang, A. Mancuso, B. Amirbekian, L. Peng, R. Sun, S. S. Shah, Z. H. Zhou, T. Ishikawa, and J. Miao, "Quantitative imaging of single, unstained viruses with coherent x rays," *Physical review letters*, vol. 101, no. 15, p. 158101, 2008.

[109] N. Loh, M. Bogan, V. Elser, A. Barty, S. Boutet, S. Bajt, J. Hajdu, T. Ekeberg, F. R. Maia, J. Schulz *et al.*, "Cryptotomography: reconstructing 3d fourier intensities from randomly oriented single-shot diffraction patterns," *Physical review letters*, vol. 104, no. 22, p. 225501, 2010.

[110] L. Strüder, S. Epp, D. Rolles, R. Hartmann, P. Holl, G. Lutz, H. Soltau, R. Eckart, C. Reich, K. Heinzinger *et al.*, "Large-format, high-speed, x-ray pnccds combined with electron and ion imaging spectrometers in a multipurpose chamber for experiments at 4th generation light sources," *Nuclear Instruments and Methods in Physics Research Section A: Accelerators, Spectrometers, Detectors and Associated Equipment*, vol. 614, no. 3, pp. 483–496, 2010.

[111] J. Bozek, "Amo instrumentation for the lcls x-ray fel," *The European Physical Journal Special Topics*, vol. 169, no. 1, pp. 129–132, 2009.

[112] S. Marchesini, H. He, H. N. Chapman, S. P. Hau-Riege, A. Noy, M. R. Howells, U. Weierstall, and J. C. H. Spence, "X-ray image reconstruction from a diffraction pattern alone," *Phys. Rev. B*, vol. 68, p. 140101, Oct 2003. [Online]. Available: http://link.aps.org/doi/10.1103/PhysRevB.68.140101

[113] R. L. Sandberg, Z. Huang, R. Xu, J. A. Rodriguez, and J. Miao, "Studies of materials at the nanometer scale using coherent x-ray diffraction imaging," *JOM*, vol. 65, no. 9, pp. 1208–1220, 2013.

[114] L.-M. Stadler, C. Gutt, T. Autenrieth, O. Leupold, S. Rehbein, Y. Chushkin, and G. GrÃ\u0152bel, "Hard x ray holographic diffraction imaging," *Physical Review Letters*, vol. 100, no. 24, p. 245503, Jun. 2008. [Online]. Available: http://link.aps.org/doi/10.1103/PhysRevLett.100.245503

[115] G. Williams, H. Quiney, B. Dhal, C. Tran, K. A. Nugent, A. Peele, D. Paterson, M. De Jonge *et al.*, "Fresnel coherent diffractive imaging," *Physical review letters*, vol. 97, no. 2, p. 025506, 2006.

[116] B. Abbey, L. W. Whitehead, H. M. Quiney, D. J. Vine, G. A. Cadenazzi, C. A. Henderson, K. A. Nugent, E. Balaur, C. T. Putkunz, A. G. Peele *et al.*, "Lensless imaging using broadband x-ray sources," *Nature Photonics*, vol. 5, no. 7, pp. 420–424, 2011.

[117] S. Witte, V. T. Tenner, D. W. Noom, and K. S. Eikema, "Ultra-broadband extreme-ultraviolet lensless imaging of extended complex structures," *arXiv preprint arXiv:1302.6064*, 2013.

[118] H. N. Chapman, "Phase-retrieval x-ray microscopy by wigner-distribution deconvolution," *Ultramicroscopy*, vol. 66, no. 3, pp. 153–172, 1996.

[119] P. Thibault, M. Dierolf, A. Menzel, O. Bunk, C. David, and F. Pfeiffer, "High-resolution scanning x-ray diffraction microscopy," *Science*, vol. 321, no. 5887, pp. 379–382, 2008.

[120] I. Peterson, B. Abbey, C. Putkunz, D. Vine, G. van Riessen, G. Cadenazzi, E. Balaur, R. Ryan, H. Quiney, I. McNulty *et al.*, "Nanoscale fresnel coherent diffraction imaging tomography using ptychography," *Optics express*, vol. 20, no. 22, pp. 24 678–24 685, 2012.

[121] O. Shapira, A. F. Abouraddy, J. D. Joannopoulos, and Y. Fink, "Complete modal decomposition for optical waveguides," *Physical review letters*, vol. 94, no. 14, p. 143902, 2005.

[122] I. Robinson and R. Harder, "Coherent x-ray diffraction imaging of strain at the nanoscale," *Nature materials*, vol. 8, no. 4, pp. 291–298, 2009.

[123] M. C. Newton, S. J. Leake, R. Harder, and I. K. Robinson, "Three-dimensional imaging of strain in a single zno nanorod," *Nature materials*, vol. 9, no. 2, pp. 120–124, 2009.

[124] W. Yang, X. Huang, R. Harder, J. N. Clark, I. K. Robinson, and H.-k. Mao, "Coherent diffraction imaging of nanoscale strain evolution in a single crystal under high pressure," *Nat Commun*, vol. 4, p. 1680, Apr. 2013. [Online]. Available: http://dx.doi.org/10.1038/ncomms2661

[125] M. Holt, R. Harder, R. Winarski, and V. Rose, "Nanoscale hard x-ray microscopy methods for materials studies*," *Annual Review of Materials Research*, vol. 43, no. 1, pp. 183–211, 2013.

[126] D. Gabor, "A new microscopic principle," *Nature*, vol. 161, no. 4098, pp. 777–778, 1948.

[127] I. McNulty, J. Kirz, C. Jacobsen, E. H. Anderson, M. R. Howells, D. P. Kern *et al.*, "High-resolution imaging by fourier transform x-ray holography," *Science*, vol. 256, no. 5059, pp. 1009–1012, 1992.

[128] S. Kikuta, S. Aoki, S. Kosaki, and K. Kohra, "X-ray holography of lensless fourier-transform type," *Optics Communications*, vol. 5, no. 2, pp. 86 – 89, 1972. [Online]. Available: http://www.sciencedirect.com/science/article/pii/0030401872900053

[129] S. Eisebitt, J. LÃ\u0152ning, W. F. Schlotter, M. LÃ¶rgen, O. Hellwig, W. Eberhardt, and J. StÃ¶hr, "Lensless imaging of magnetic nanostructures by x-ray spectro-holography," *Nature*, vol. 432, no. 7019, pp. 885–888, Dec. 2004. [Online]. Available: http://www.nature.com/nature/journal/v432/n7019/abs/nature03139.html

[130] T. Latychevskaia, J.-N. Longchamp, and H.-W. Fink, "When holography meets coherent diffraction imaging," *Optics express*, vol. 20, no. 27, pp. 28 871–28 892, 2012.

[131] T. Popmintchev, M.-C. Chen, D. Popmintchev, P. Arpin, S. Brown, S. Ališauskas, G. Andriukaitis, T. Balčiunas, O. D. Mücke, A. Pugzlys *et al.*, "Bright coherent ultrahigh harmonics in the kev x-ray regime from mid-infrared femtosecond lasers," *Science*, vol. 336, no. 6086, pp. 1287–1291, 2012.